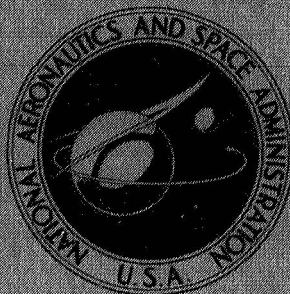


NASA TECHNICAL
MEMORANDUM



NASA TM X-1793

NASA TM X-1793

COPY

ANALYTICAL EVALUATION OF SPACE STORABLE PROPELLANTS FOR UNMANNED JUPITER AND SATURN ORBITER MISSIONS

by Jon C. Oglebay, Gary D. Sagerman, and Harold H. Valentine

Lewis Research Center

Cleveland, Ohio

NASA TM X-1793

ANALYTICAL EVALUATION OF SPACE STORABLE PROPELLANTS FOR
UNMANNED JUPITER AND SATURN ORBITER MISSIONS

By Jon C. Oglebay, Gary D. Sagerman,
and Harold H. Valentine

Lewis Research Center
Cleveland, Ohio

NATIONAL AERONAUTICS AND SPACE ADMINISTRATION

For sale by the Clearinghouse for Federal Scientific and Technical Information
Springfield, Virginia 22151 - CFSTI price \$3.00

ABSTRACT

An analytical study was performed to evaluate the potential application of space storable propellants to unmanned planetary orbit missions. The study concentrated on retrostages for Jupiter and Saturn orbiter missions. The performance capabilities and space storage characteristics of Earth storable, space storable, and deep cryogenic stages are compared. Mission times up to 1500 days were considered, and all results shown are based on nonvented propellant storage over the entire mission time.

ANALYTICAL EVALUATION OF SPACE STORABLE PROPELLANTS FOR

UNMANNED JUPITER AND SATURN ORBITER MISSIONS

by Jon C. Oglebay, Gary D. Sagerman,
and Harold H. Valentine

Lewis Research Center

SUMMARY

An analytical study was performed to evaluate the potential application of space storable propellants to unmanned planetary orbit missions. The study concentrated on retrostages for Jupiter and Saturn orbiter missions. The performance capabilities and space storage characteristics of Earth storable, space storable, and deep cryogenic stages are included and compared. The launch vehicles considered were uprated Saturn I Centaur, 260-inch solid/S-IVB/Centaur, Saturn V, and Saturn V/Centaur. Mission times ranged from 500 to 1500 days.

The results indicate that for the missions considered the space storable propellants can be stored nonvented over the entire mission time independent of stage orientation by utilizing multilayer insulation and low conductivity tank supports. Utilizing payload to the Sun orientation plus shadow shields results in storability characteristics for the deep cryogenics that are similar to those of the space storables.

The results also indicate that both the space storable and the deep cryogenic stages offer a payload advantage over Earth storable stages when compared on a fixed velocity increment (ΔV) basis. However, regardless of the propellant combination selected, the payload level can be significantly influenced by changes in trip time, periapsis altitude, and orbit eccentricity. Therefore, the absolute advantage of the more energetic propellant combinations over Earth storables is largely determined by how rigidly the payload planner constrains the mission parameters.

INTRODUCTION

Most space propulsion systems utilized to date or presently under development are based on the use of liquid or solid Earth storable propellants. At the present time, there is considerable interest both within NASA and in industry regarding the application of "space storable" propellants to future manned and unmanned missions. The term "space storable" as utilized herein applies to that class of liquid propellants whose nor-

mal boiling points fall in the range of approximately 88.9 to 183.3 K. For the analytical study documented by this report, methane-flox (82.5 percent fluorine - 17.5 percent oxygen) was selected as a representative space storable propellant combination. The space storable propellants are more energetic than the Earth storables. This fact can affect the launch vehicle requirements for some missions. Also, even though the space storables are less energetic than the deep cryogenics (i.e., those combinations involving hydrogen), they exhibit higher normal boiling point temperatures and give higher propellant bulk densities than the deep cryogenics - both of which affect the propellant storability.

In order to evaluate the potential application of space storable propellants to unmanned planetary orbit missions, an analytical study was performed. The study concentrated on retrostages for Jupiter and Saturn orbiter missions. These stages were assumed to perform only the braking maneuver at the planet and were not used to provide any of the injection ΔV requirement. The performance capabilities and space storage characteristics of Earth storable, space storable, and deep cryogenic stages are included and compared. All results shown assume nonvented propellant storage over the entire space portion of the mission from injection to retro into planetary orbit.

MISSION ANALYSIS

Energy Requirements

The velocity requirements for the planetary missions discussed in this report were generated assuming that the planets are in circular coplanar orbits around the Sun. Consequently, the data, although useful for illustrating the general requirements and trends, can be somewhat in error for a specific planetary opportunity.

The general behavior of the retrovelocity requirements for Jupiter and Saturn orbiter missions is shown in figures 1 to 4. In figure 1, retrovelocity increment (ΔV_r) is plotted as a function of apoapsis radius ratio (apoapsis radius/planet radius) for a periapsis radius ratio (periapsis radius/planet radius) of 3.0. Data for the minimum energy trip and for a mission with a flight time about half that of the minimum energy trip are shown. The required injection velocity at Earth for each of the specified trip times is also given. The injection velocity used herein is the actual velocity of the injected mass assuming injection occurs at 185 kilometers. The figure indicates that, for a constant periapsis radius, ΔV_r may be reduced greatly by accepting higher apoapsis radii (more eccentric orbits) or longer trip times. Figure 2 shows similar data for Saturn missions. The same general observations may be made for Saturn as for Jupiter although the slopes of the curves are somewhat different.

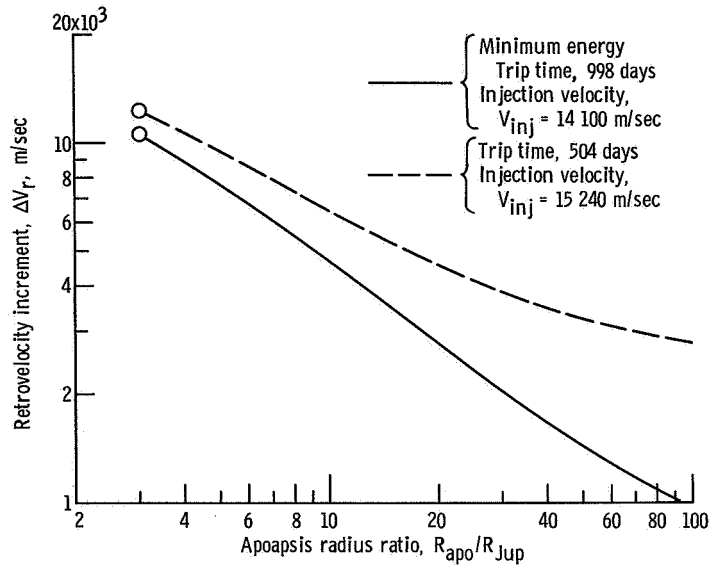


Figure 1. - Retrovelocity increment plotted against apoapsis radius ratio for Jupiter orbiters. Periapsis radius, $3.0R_{Jup}$.

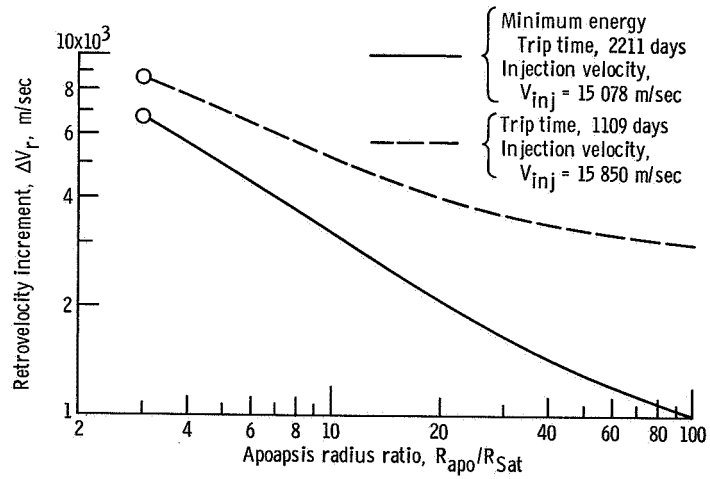


Figure 2. - Retrovelocity increment plotted against apoapsis radius ratio for Saturn orbiters. Periapsis radius, $3.0R_{Sat}$.

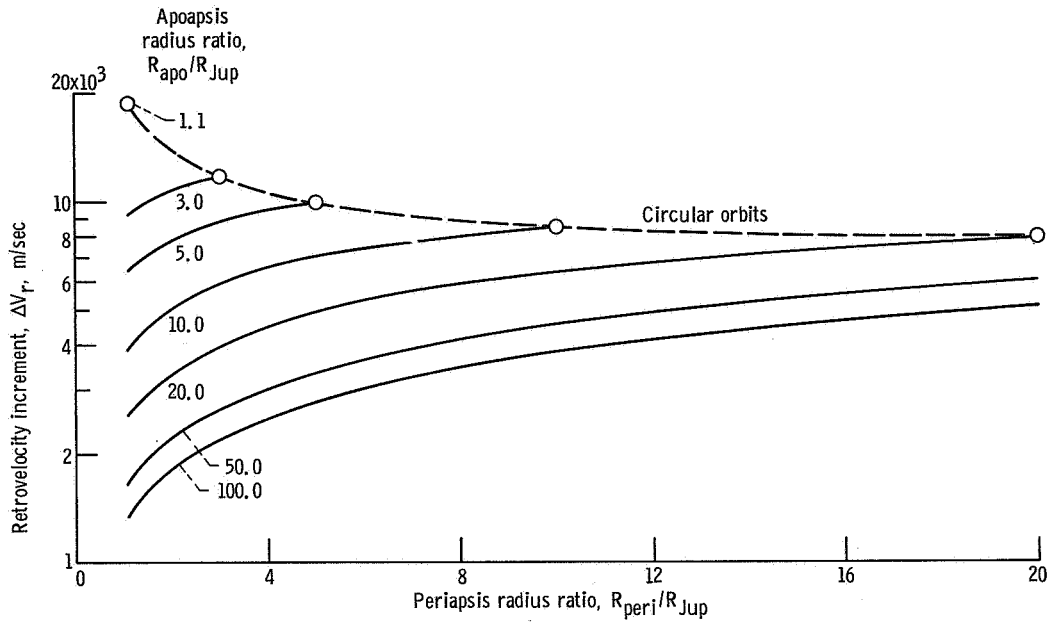


Figure 3. - Jupiter orbiter retrovelocity increment plotted against periapsis radius ratio for several apoapsis radius ratios. Trip time, 554 days.

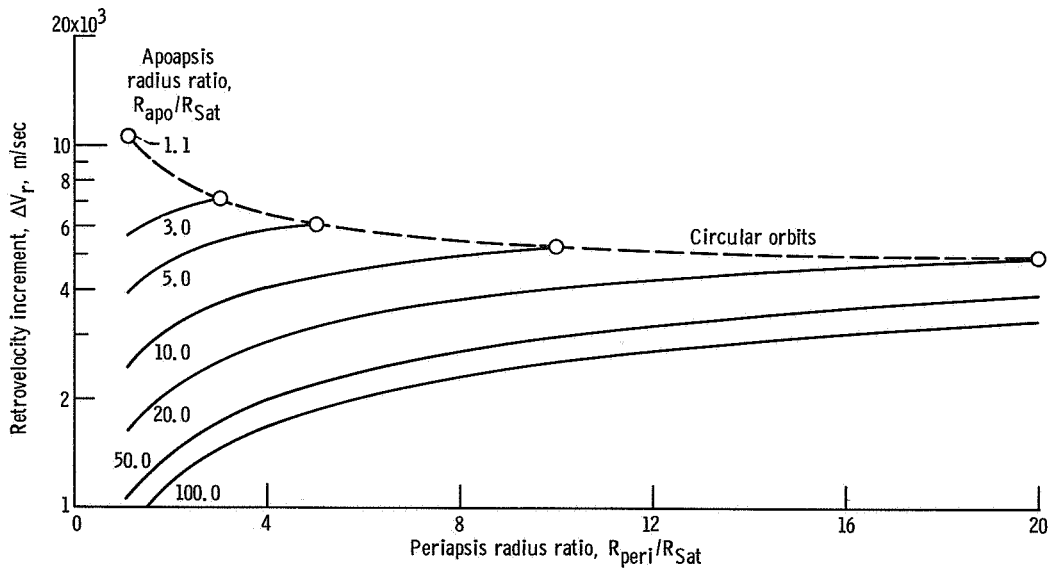


Figure 4. - Saturn orbiter retrovelocity increment plotted against periapsis radius ratio for several apoapsis radius ratios. Trip time, 1532 days.

Figures 3 and 4 show the effect of periapsis radius on the retrovelocity requirements for Jupiter and Saturn, respectively. For a typical trip time to each planet, ΔV_r is plotted against periapsis radius ratio for several values of apoapsis radius ratio. The dashed line indicates circular orbits where periapsis radius is equal to apoapsis radius. It is evident from the figures that if circular orbits are required, the higher orbits require the lesser retro ΔV 's in the range shown. However, if the apoapsis radius is held fixed, ΔV_r may be reduced by lowering the periapsis.

Various studies of interplanetary missions have utilized orbits which approach the target planet to as close as 0.1 planet radii (periapsis radius ratio, 1.1). It is felt, however, that such a low periapsis may not be a good choice for early Jupiter and Saturn missions. Radio emission from Jupiter has led to hypotheses that strong trapped radiation belts extending out to about three planet radii may exist about the planet. In the case of Saturn, it is not known if radiation belts are present. However, the rings of Saturn extend out to approximately two and one-half planet radii. Since each of these situations might cause damage to or somehow affect the performance of a spacecraft at a low altitude, it was decided to limit consideration in this study to orbits with a periapsis of 3.0 planet radii.

Mission velocity requirements are presented as functions of interplanetary trip time to Jupiter and Saturn in figures 5 and 6, respectively. The periapsis radius ratio of 3.0 is used in the figures. Retro ΔV is shown for several apoapsis radii for 400- to 998-day Jupiter trips in figure 5. The required injection velocity at Earth for each trip time

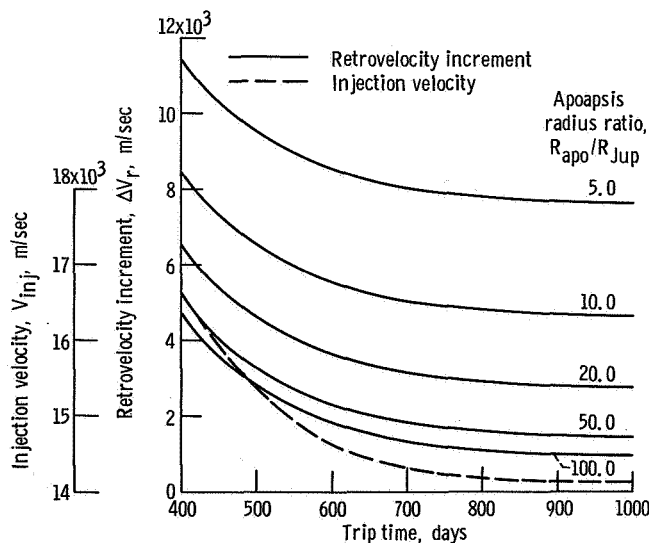


Figure 5. - Injection velocity and retrovelocity increment plotted against trip time to Jupiter for several apoapsis radius ratios. Periapsis radius, $3.0R_{Jup}$.

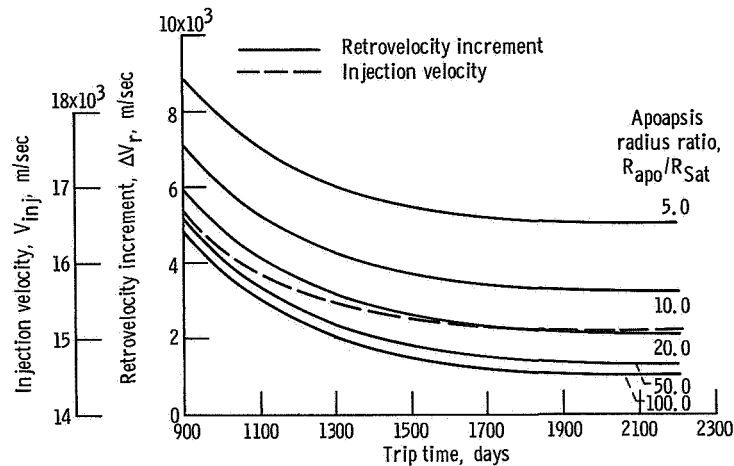


Figure 6. - Injection velocity and retrovelocity increment plotted against trip time to Saturn for several apoapsis radius ratios. Periapsis radius, $3.0R_{Sat}$.

is also shown. The curves show that both ΔV and injection velocity increase very rapidly for trip times of less than 500 to 600 days. Similar data are shown in figure 6 for trip times to Saturn of 900 to 2211 days. In this case, the velocity requirements increase rapidly for trip times below 1200 to 1300 days.

Launch Vehicle Performance

In order to provide a range of launch vehicle capability, four launch vehicles were considered in this study. Their performance is summarized in figure 7. The data for the uprated Saturn I/Centaur, Saturn V, and Saturn V/Centaur are based on present hardware although some future modifications and improvements might be expected. The 260-inch solid/S-IVB/Centaur vehicle is based on a full-length 260-inch solid first stage (1.54×10^6 kg propellant mass) with present S-IVB and Centaur upper stages.

The payload data of figure 7 are replotted in figures 8 and 9 as functions of trip time for Jupiter and Saturn missions, respectively. The injected mass shown is the total package placed on the transfer conic at Earth by the launch vehicle. This includes both the retropropulsion module and the orbiter spacecraft or payload. Although for some configurations the retropropulsion module and orbiting payload could be physically integrated into one overall spacecraft, they will be treated as two distinct modules in the present study. For brevity, the orbiting spacecraft or final payload is referred to as simply the payload.

In order to determine the adequacy of a given launch vehicle for the missions considered here, it is first necessary to establish a desired payload level. The payload

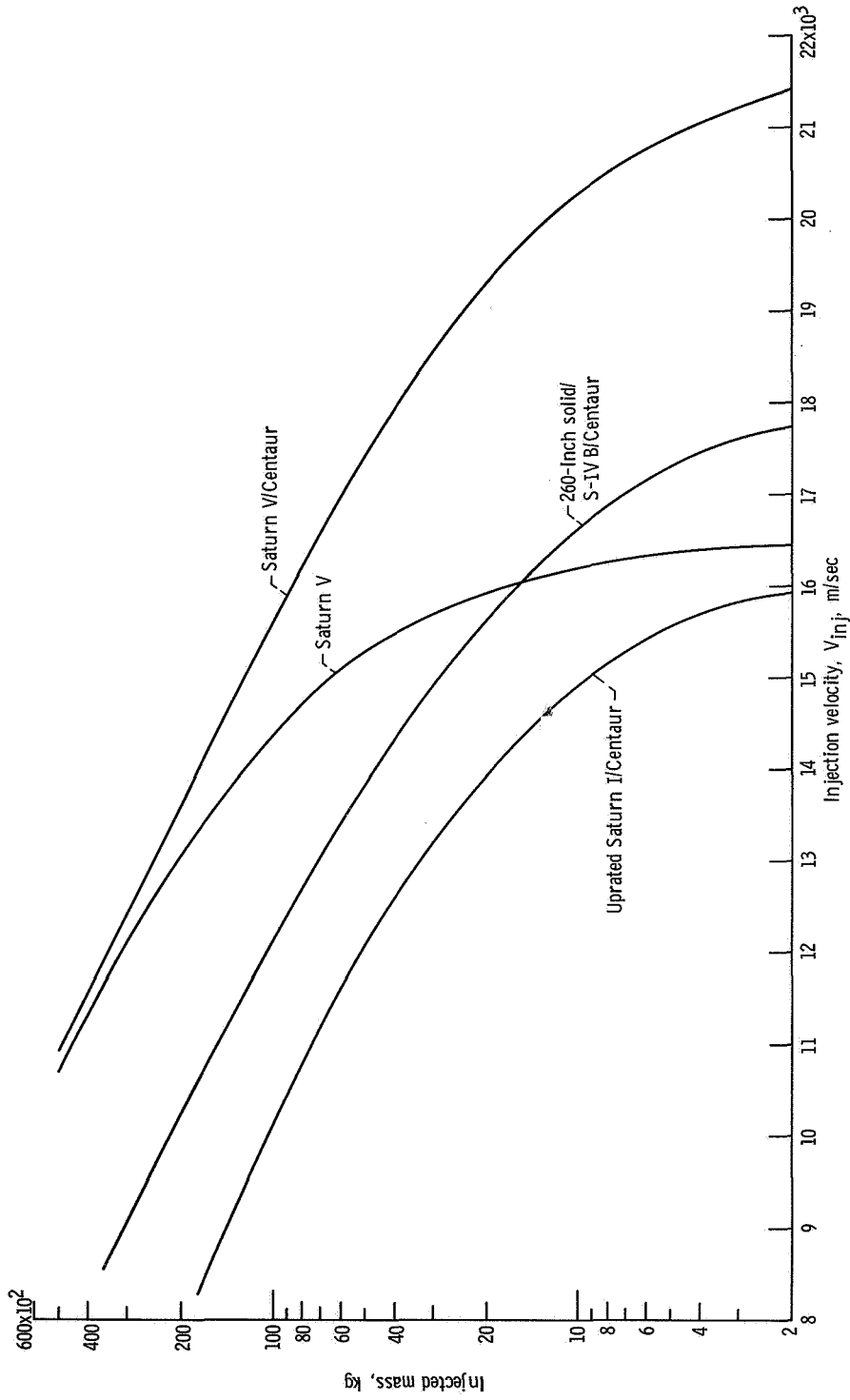


Figure 7. - Payload plotted against characteristic velocity for several launch vehicles. Injection altitude, 185 kilometers.

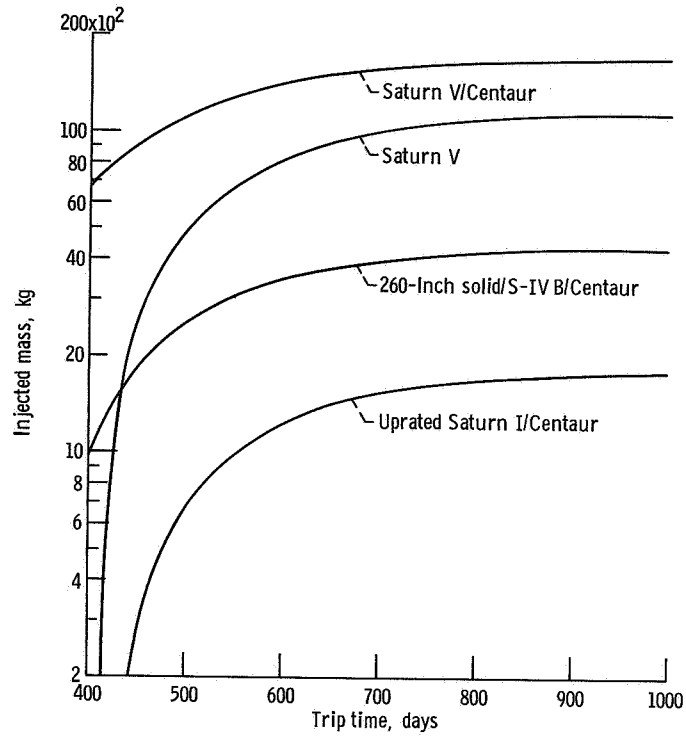


Figure 8. - Injected mass plotted against trip time to Jupiter for several launch vehicles.

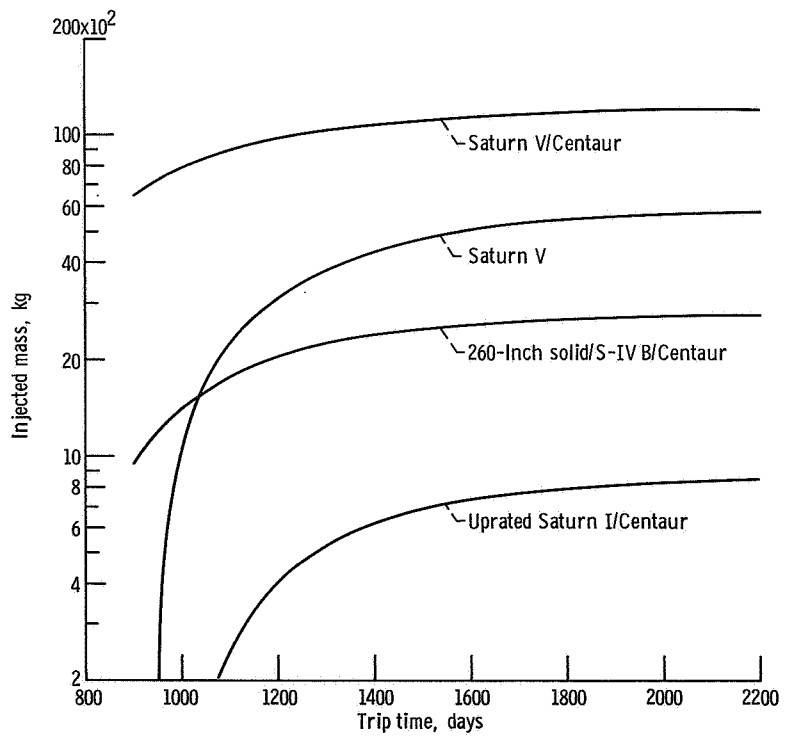


Figure 9. - Injected mass plotted against trip time to Saturn for several launch vehicles.

levels that have been considered in the literature for outer planet orbiters range from a few hundred to 1000 kilograms. Certainly, at the lower levels one would not consider the use of space storable retropropulsion modules. Small solid or liquid monopropellant systems would be adequate. It is only when larger payloads or more energetic orbits are considered that space storable or cryogenic propellants enter the picture. In this study, we have chosen 907 kilograms as representative of the payload level for which the space storable propellants might be used. Typically for a planetary orbiter mission, at least half of the mass injected on the transfer conic is required to provide the retropropulsion, leaving half or less as payload. Therefore, a launch vehicle injection capability of at least 1814 kilograms is required for the missions of interest here.

For the Jupiter mission (fig. 8), the uprated Saturn I/Centaur injected mass approaches the minimum 1814 kilograms only at the longest trip times. This was considered too restrictive a situation and the uprated Saturn I/Centaur was not considered further. For the 260-inch solid launch vehicle, trip times of 500 to 700 days appear reasonable. Little is gained by going to longer trip times; and below 500 days, the injected mass drops rapidly. If higher injected masses are desired, either the Saturn V or Saturn V/Centaur can be used. For the Saturn V, trip times of 500 to 700 days again appear to be a reasonable choice from a launch vehicle standpoint. As trip times near or below 500 days are considered, the Saturn V/Centaur becomes more appropriate. (Note, however, that this results in heavy masses on the Centaur stage which would require strengthening its structure. This has not been accounted for in the present study.)

Launch vehicle performance for Saturn missions is presented in figure 9. Again, the uprated Saturn I/Centaur is inadequate for the payload levels considered. For the 260-inch solid vehicle and the Saturn V, trip times as low as 1500 days could be selected without a serious loss in injected mass. With the Saturn V/Centaur, trip times as short as 1000 days appear reasonable.

STAGE SIZING AND CHARACTERISTICS

In order to proceed with the preliminary design of appropriate retrostages, it is necessary to establish the approximate stage sizes (propellant loadings) desired. To determine reasonable stage sizes, a preliminary overall mission calculation was made assuming a pressure-fed Earth storable retropropulsion module. A specific impulse of 305 seconds (2991 (N)(sec)/kg) and a mass fraction of 0.80 were selected for the calculation. Based on these calculations, a retrostage propellant load of 6350 kilograms was selected as typical for Jupiter and Saturn missions using the Saturn V or Saturn V/Centaur. For missions using the 260-inch solid/S-IVB/Centaur launch vehicle, a retrostage propellant load of 1360 kilograms was selected for preliminary design purposes.

Propulsion

Listed in table I are some of the engine performance characteristics assumed for the various propellant combinations considered. Chamber pressure and nozzle expansion ratio were not varied in the study. Rather, values were selected which, based on previous inhouse studies, should be near optimum for the stage sizes under consideration.

Similarly, the specific impulse values indicated are considered representative for the various propellant combinations.

The variation of engine mass with thrust assumed for the study is presented in figure 10. The pump-fed curve was used for all pump-fed stages regardless of the propellant combination. Although, in reality, some variations in engine mass with propellant

TABLE I. - ENGINE CHARACTERISTICS

[Nozzle expansion ratio, 60.]

Propellant combination	Chamber pressure, N/cm ²	Mixture ratio	Specific impulse, sec (N)(sec)/kg
Hydrogen-fluorine	345	12	460 (4511)
Hydrogen-oxygen	345	5	444 (4354)
Methane-flox	345	5	400 (3923)
Methane-flox	69	5	385 (3776)
Monomethyl hydrazine - mixed oxides of nitrogen	345	2.00	320 (3138)
Monomethyl hydrazine - mixed oxides of nitrogen	69	1.65	305 (2991)

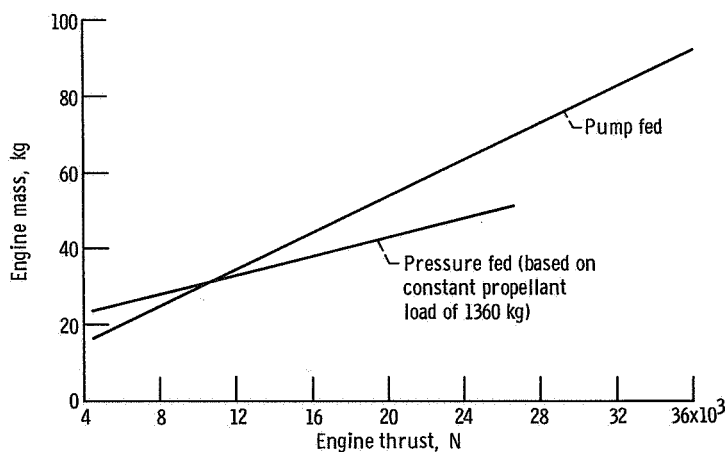


Figure 10. - Variation of engine mass with thrust.

combinations would be expected, the magnitude of such variations would be small for the thrust range considered and would have an insignificant effect on the study results. Regenerative cooling was assumed for the pump-fed engines while ablative cooling was selected for the pressure-fed engines.

Pressure-fed stages were only considered for the smaller (nominal 1360-kg propellant) stage size. The mass of an ablative engine increases with increases in thrust level and/or burning time. However, for a fixed propellant mass stage, increasing the thrust level results in a proportional decrease in burning time. Therefore, in figure 10, the slope of the engine mass against thrust curve for the pressure-fed engines is less than that of the pump-fed engines which are insensitive to burning time.

The pressure-fed engine masses are based on ablative cooling to a nozzle expansion ratio of 15 and radiation cooling from there to the nozzle exit.

The sensitivity of payload to thrust level is presented in figure 11 for the larger space storable stages suitable for use with either the Saturn V or Saturn V/Centaur launch vehicles. Results are presented for three missions: two Jupiter missions using different launch vehicles, and a Saturn mission using the Saturn V/Centaur. The results indicate little variation in payload capability with variations in thrust level. A thrust level of 22 250 newtons is near optimum for all three missions, and this value was used for all of the larger pump-fed stages.

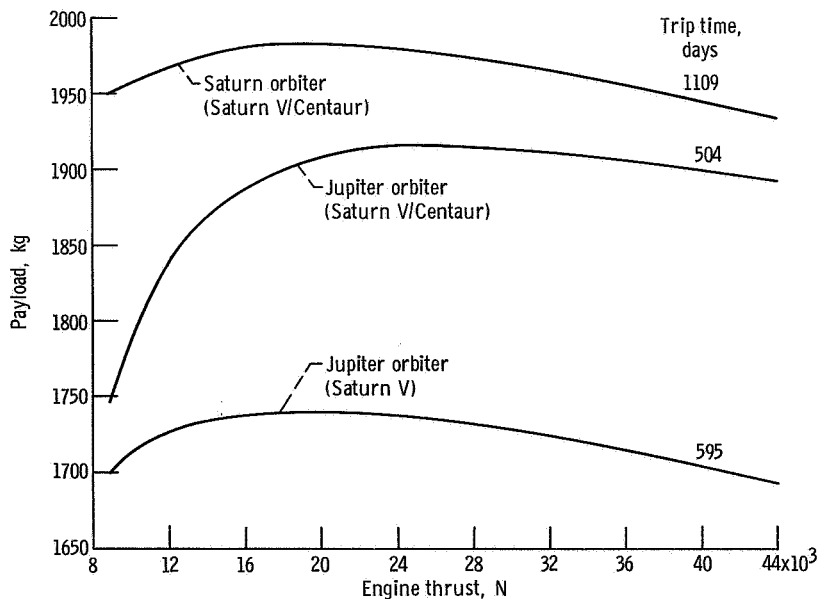


Figure 11. - Effect of retrothrust level on orbiter payload; methane-flox retrostages.

Similar information, but for the smaller stages sized for use on the 260-inch solid vehicle, is presented in figure 12. Payload capability plotted against thrust level is shown for a Jupiter orbiter mission for both pump-fed and pressure-fed space storable stages. Again, the results are quite insensitive to thrust level. A thrust level of 6675 newtons appears optimum for either pump-fed or pressure-fed stages. Similar data were generated for Saturn orbiters for Earth storable as well as space storable stages. The results were similar: a thrust level of 6675 newtons was good for all the small stages. Therefore, this thrust level was used in generating all the subsequent performance data for the small stages.

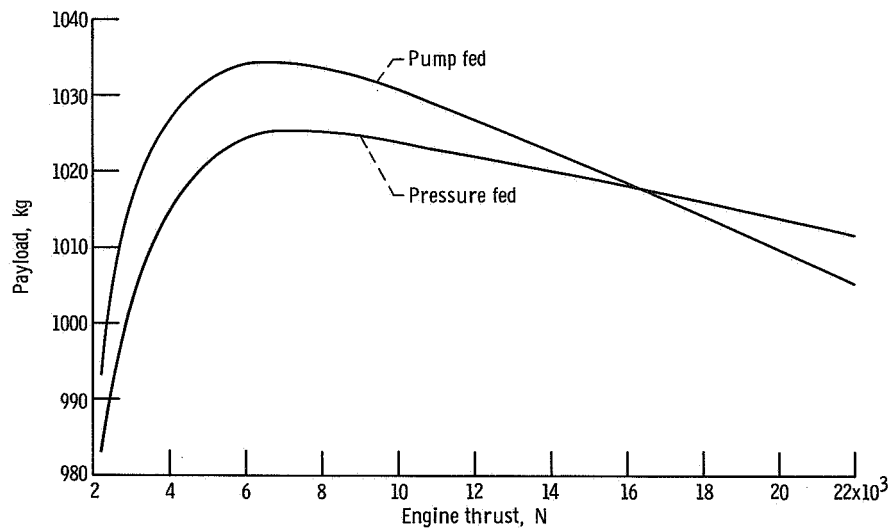


Figure 12. - Effect of retrothrust level on Jupiter orbiter payload; methane-flox retrostages. 260-Inch solid/S-IV B/Centaur; trip time, 550 days.

Pressurization

The pressurization system weights were based on the use of a simple helium blow-down system for the pressurization and expulsion of all tanks except the fuel tanks of the pump-fed stages. The helium was stored initially at 294.4 K and 2.8×10^3 newtons per square centimeter (N/cm^2) in a titanium bottle. For the fuel tanks of the pump-fed stages, it was assumed that while initial pressurization would be with helium, vaporized fuel could be withdrawn downstream of the cooling jacket for pressurization during expulsion.

The pressurization system masses are directly affected by the operating pressures of the tanks. These, in turn, are dependent on the engine requirements, the nominal propellant heating histories, and the tolerance to variations in the thermal parameters that one chooses to design for.

Meteoroid Protection

At the present time, the understanding of the deep space interplanetary meteoroid environment is so vague that no meaningful evaluation of the protection requirements can be made. The protection requirements depend on the meteoroid particle density, number density, and velocity distributions with respect to distance from the Sun along with penetration criteria and spacecraft hull bumper efficiency. Depending on what assumptions one makes regarding these variables, estimates of the protection requirements for the vehicle sizes considered here range from a few percent of the payload capability to over 100 percent of the payload capability.

Certainly, the protection necessary is a function of the exposed surface area as well as mission time. On this basis, the hydrogen-oxygen stage considered herein (largest surface area) requires about four times the protection mass of the Earth storable stage considered (smallest surface area). Whether or not this increase is significant from the standpoint of absolute stage performance cannot yet be answered.

As an example, for an 1100-day mission to Saturn, the hydrogen-oxygen stage requires 258 kilograms for meteoroid protection, while the Earth storable stage needs only 60 kilograms. This is based on the following assumptions:

(1) Cometary flux is obtained from Pegasus data (ref. 1) with a $1/\sqrt{R}$ distribution, where R is the distance from the Sun in astronomical units.

(2) The protection is comprised of aluminum face sheets placed 5.1 centimeters apart and filled with 0.032 gram per cubic centimeter foam which yield a bumper factor of 5 (ref. 2).

(3) The probability of no backsheet penetrations is 0.99.

Assuming a bumper factor of 1 (i. e., armor-plating the tanks) would nearly eliminate the payload capability of the hydrogen-oxygen stage. If a bumper factor of, say, 10 is achieved, the meteoroid hazard is relegated to a minor problem based on the assumptions used.

As indicated earlier, more definitive information is necessary to assess accurately the protection requirements. Therefore, no meteoroid protection penalty was imposed on any of the stages considered herein.

Residuals

For each stage considered, an allowance of 1 percent of the stage propellant mass was included in the stage jettison mass to account for liquid and gaseous residuals. An additional 2 percent of the fuel mass was included as a fuel bias in lieu of a propellant utilization system.

TABLE II. - MASS BREAKDOWNS AND MASS FRACTIONS FOR THE 6350-KILOGRAM STAGES

	Propellant combination					
	Methane-flox	Methane-flox	Hydrogen-oxygen	Hydrogen-fluorine	Monomethyl hydrazine - mixed oxides of nitrogen	
	Configuration			Two-tank	Two-tank	Common bulkhead
Common bulkhead	Common bulkhead	Two-tank	Two-tank	Two-tank	Two-tank	Common bulkhead
Maximum tank pressure, N/cm ²						
28(fuel)-69(oxidant)	28(fuel)-28(oxidant)	28(fuel)-41(oxidant)	41(fuel)-41(oxidant)	41(fuel)-41(oxidant)	41(fuel)-41(oxidant)	28(fuel)-52(oxidant)
Mass, kg						
Structure:	194.6	140.0	176.1	451.3	326.5	172.4
Fuel tank	39.6	39.6	27.6	188.3	94.3	43.6
Oxidant tank	95.0	40.4	35.5	67.4	58.3	67.1
Tank supports	---	---	33.0	52.7	39.1	---
Basic structure	60.0	60.0	80.0	134.6	126.6	61.7
Shadow shields	---	---	---	8.2	8.2	---
Propellant system	22.7	22.7	22.7	22.7	22.7	22.7
Pressurization system:	89.0	45.0	45.0	70.3	55.5	40.8
Pressurant	9.1	4.1	4.1	6.8	5.4	3.6
Bottle	70.8	31.8	31.8	54.4	41.0	28.1
Hardware	9.1	9.1	9.1	9.1	9.1	9.1
Engine	59.0	59.0	59.0	59.0	59.0	59.0
Range safety	6.8	6.8	6.8	6.8	6.8	6.8
Instrumentation and harnessing	27.2	27.2	27.2	27.2	27.2	27.2
Separation system	11.3	11.3	11.3	11.3	11.3	11.3
Insulation	52.2	52.2	68.0	98.0	90.3	45.4
Contingency (10 percent)	46.3	36.4	41.6	74.7	60.0	38.6
Dry mass	509.1	400.6	457.7	821.2	659.3	424.4
Residuals	84.7	84.7	84.7	84.7	78.3	111.4
Jettison mass	593.8	485.3	542.4	905.9	732.6	535.8
Useful propellant	6350.0	6350.0	6350.0	6350.0	6350.0	6350.0
Stage loaded mass	6943.8	6835.3	6892.4	7255.9	7082.6	6885.8
Mass fraction	0.91	0.93	0.92	0.88	0.90	0.92

Stage Mass Tables

The mass breakdown and mass fraction for each of the stages considered are presented in tables II and III. All of the stages were treated as propulsion modules rather than complete stages. Therefore, the guidance, attitude control, electrical, and instrumentation requirements were assumed to be provided by or integrated with the payload. However, a mass is charged to the stages to account for instrumentation and harnessing normally associated with the propulsion system.

Table II includes all of the 6350-kilogram propellant load stages. The mass frac-

TABLE III. - MASS BREAKDOWNS AND MASS FRACTIONS FOR THE 1360-KILOGRAM STAGES

	Propellant combination		
	Methane-flox	Methane-flox	Monomethyl hydrazine - mixed oxides of nitrogen
	Configuration		
	Two-tank pressure-fed	Two-tank pump-fed	Two-tank pressure-fed
	Maximum tank pressure, N/cm ²		
	110(fuel)-138(oxidant)	28(fuel)-69(oxidant)	110(fuel)-138(oxidant)
	Mass, kg		
	Structure:	107.4	86.7
Fuel tank	20.0	9.8	21.3
Oxidant tank	23.0	12.5	29.0
Tank supports	26.3	26.3	24.5
Basic structure	38.1	38.1	44.4
Shadow shields	----	----	----
Propellant system	11.3	11.3	11.3
Pressurization system:	69.0	17.3	40.8
Pressurant	6.8	0.9	3.6
Bottle	53.1	7.3	28.1
Hardware	9.1	9.1	9.1
Engine	26.3	21.8	26.3
Range safety	6.8	6.8	6.8
Instrumentation and harnessing	27.2	27.2	27.2
Separation system	6.8	6.8	6.8
Insulation	23.6	23.6	23.1
Contingency (10 percent)	27.8	20.2	26.1
Dry mass	306.2	221.7	287.7
Residuals	18.1	18.1	23.9
Jettison mass	324.3	239.8	311.6
Useful propellant	1360.0	1360.0	1360.0
Stage loaded mass	1684.3	1599.8	1671.6
Mass fraction	0.81	0.85	0.81

TABLE IV. - SUMMARY OF VARIOUS STAGES ANALYZED

Propellant load, kg	Propellant combination	Stage configuration	Tank materials	Structural materials	Stage coast orientation
6350	Methane-flox	Common bulkhead and nested tanks	2219-T81 Al 301-1/2 hard stainless steel Electro-formed Ni	2219-T81 Al 301-1/2 hard stainless steel Fiber glass	Velocity vector Engine to Sun Payload to Sun
6350	Methane-flox	Two-tank	2219-T81 Al Electro-formed Ni	2219-T81 Al 301-1/2 hard stainless steel Fiber glass	Engine to Sun Payload to Sun
6350	Methane-flox	Four-tank	2219-T81 Al	2219-T81 Al Fiber glass	-----
1360	Methane-flox	Two-tank	2219-T81 Al	2219-T81 Al Fiber glass	Payload to Sun
1360	Methane-flox	Common bulkhead ^a		-----	Velocity vector Payload to Sun
6350	Hydrogen-oxygen	Two-tank	2219-T81 Al	2219-T81 Al Fiber glass	Payload to Sun
6350	Hydrogen-fluorine	Two-tank	2219-T81 Al	2219-T81 Al Fiber glass	Payload to Sun
6350	Monomethyl hydrazine - mixed oxides of nitrogen	Common bulkhead	301-1/2 hard stainless steel	301-1/2 hard stainless steel 2219-T81 Al	Payload to Sun
1360	Monomethyl hydrazine - mixed oxides of nitrogen	Two-tank	2219-T81 Al	2219-T81 Al	Payload to Sun

^aNo detailed structural design was conducted on this configuration, but tankage was sized in order to conduct a thermal comparison with the 6350-kg common bulkhead configuration.

tions range from 0.88 for the hydrogen-oxygen stage to 0.93 for the methane-flox common bulkhead stage utilizing a low oxidant tank pressure.

The stage masses and mass fractions for the 1360-kilogram propellant load stages are presented in table III. The mass fractions are 0.81 and 0.85, respectively, for the pressure-fed and pump-fed methane-flox stages. The Earth storable stage also has a mass fraction of 0.81.

The stage masses given in tables II and III resulted from structural and thermal control analyses. These analyses considered various tank configurations, materials, and stage coast orientations to obtain a relative comparison of the stage masses and propellant storability characteristics. The stages which appear in the tables are those selected for performance comparisons based on the results of the previous analyses. A summary of the various cases analyzed is given in table IV, while a detailed discussion is presented in the following sections of the report.

STAGE DESIGN

Configurations, Structures, and Materials

A configuration and preliminary structural design study was undertaken to estimate stage masses for performance calculations and to select a feasible configuration based on stage inert mass, propellant heating, and structural integrity. The study was made for one space storable and two deep cryogenic propellant combinations: methane-flox, hydrogen-oxygen, and hydrogen-fluorine. For purposes of comparison, an Earth storable propellant combination, monomethyl-hydrazine (MMH) and mixed oxides of nitrogen (MON), was also included. Stages were sized for a 6350-kilogram propellant load for each of the four propellant combinations, and a 1360-kilogram propellant load stage was also sized for the Earth storable and the methane-flox combinations. Thus, six basic stages were studied.

All of the proposed configurations were constrained to state-of-the-art materials and fabrication. The basic tank material considered was 2219-T81 aluminum.

At the present time, insufficient experience exists to determine if tank corrosion will be a problem in storing flox in aluminum tanks for long periods of time in space. Based on the data available in references 3 and 4, however, it appears that, by precluding moisture from the tank and by minimizing the HF (hydrogen-fluoride) content of the flox, no significant corrosion should occur. Therefore, in determining flox tank weights using aluminum, no allowance for corrosion was made; however, because of the possible corrosion problem with aluminum, alternate tank materials, 301-1/2 hard stainless steel and cold-worked electro-formed nickel, were considered. As will be shown, stage jettison mass was fairly insensitive to tank material selection.

The minimum fabrication thicknesses assumed for the tank materials were the following:

Material	Minimum gage, cm
301-1/2 hard stainless steel	0.0356
2219-T81 aluminum	.0762
Electro-formed nickel	.0356

The design load for the propellant tanks was 1.1 times maximum expected tank pressure, and the tanks were sized assuming a 10-percent ullage volume. The materials selected for structural members were 2219-T81 aluminum, 301-1/2 hard stainless steel, and epoxy laminates reinforced with 181 style S fiber glass fabric. The fiber glass structural material is attractive for thermal isolation of cryogenic propellants. The safety factor on material ultimate stress was 1.25 while the design load factors for sizing the structural members were assumed as follows:

Condition	Gravity load factor (limit)	
	Axial	Lateral
Maximum q regime	2.5	1.5
Maximum booster acceleration	6.5	.5

The diameters of all the retrostages considered were smaller than those of the launch vehicles considered. Therefore, it was assumed that during launch the retrostage as well as the payload would be shrouded on the launch vehicle.

The propellant combinations, materials, load factors, and constraints used for the preliminary design activity have now been summarized. The following sections, which are organized by propellant combinations, describe the stages in more detail.

Methane-Flox Propellant Combinations

For the larger stage size, 6350 kilograms, a pump-fed common bulkhead configuration (fig. 13) having the following characteristics was chosen for the nominal case. The tank material was 2219-T81 aluminum. Fiber glass struts were used in the payload

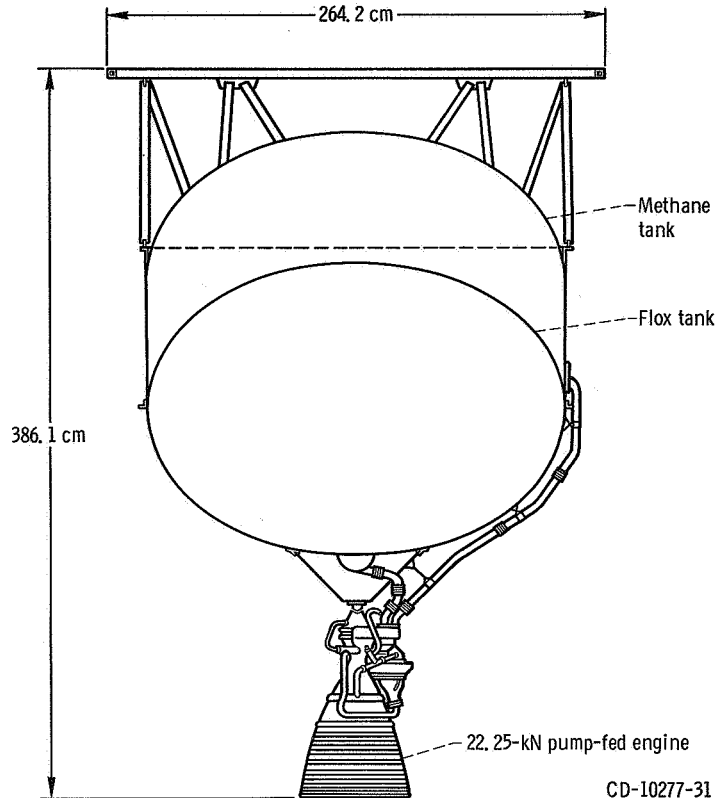


Figure 13. - Schematic of 6350-kilogram methane-flox common bulkhead retrostage.

adapter to reduce thermal conduction into the propellants. The fuel and oxidant tanks were designed for 28 and 69 N/cm² maximum ullage pressures, respectively. These pressures were selected from propellant heating and engine net positive suction head considerations.

To determine their effect on stage mass, other tank materials and pressures were considered for the nominal configuration. These were as follows:

- (1) 2219-T81 aluminum tanks, both at 28 N/cm² ullage pressure
- (2) 301-1/2 hard stainless steel methane tank, 28 N/cm² ullage pressure; electro-formed nickel flox tank, 69 N/cm² ullage pressure
- (3) Stainless steel and nickel tanks, both at 28 N/cm² ullage pressure

Design summaries of the four common bulkhead configurations (nominal and the previous three) are shown in table V along with other designs to be described subsequently. The tankage masses shown in this table are the following:

- (1) Membrane mass of the tank considering only the design thickness
- (2) Local strengthening-allowable mass for strengthening of weld areas
- (3) Total - the sum of the first two

The first four columns summarize the common bulkhead configurations.

TABLE V. - DESIGN SUMMARY FOR THE 6350-KILOGRAM METHANE-FLOX CONFIGURATIONS

	Configuration														
	Common bulkhead						Nestled tank						Two-tank		Four-tank
	High pressure (Al tanks)	Low pressure (Al tanks)	High pressure (stainless steel and Ni tanks)	Low pressure (stainless steel and Ni tanks)	Low pressure (Al tanks)	Low pressure (stainless steel and Ni tanks)	Low pressure (Al tanks)	Low pressure (stainless steel and Ni tanks)	Low pressure (Al tanks)	Low pressure (Al and Ni tanks)	Low pressure (Al tanks)	Low pressure (Al and Ni tanks)	Low pressure (Al tanks)	Low pressure (Al tanks)	
Fuel tank:	2219-T81 Al	2219-T81 Al	301-1/2 hard stainless steel	301-1/2 hard stainless steel	2219-T81 Al	2219-T81 Al	301-1/2 hard stainless steel	2219-T81 Al	2219-T81 Al	2219-T81 Al	2219-T81 Al	2219-T81 Al	2219-T81 Al	2219-T81 Al	
Material	2.8x10 ⁴	2.8x10 ⁴	6.9x10 ⁴	6.9x10 ⁴	2.8x10 ⁴	2.8x10 ⁴	6.9x10 ⁴	2.8x10 ⁴	2.8x10 ⁴	2.8x10 ⁴	2.8x10 ⁴	2.8x10 ⁴	2.8x10 ⁴	2.8x10 ⁴	
Working stress, N/cm ²	28	28	28	28	28	28	28	28	28	28	28	28	28	28	
Ullage pressure, N/cm ²	0.0762	0.0762	0.0356	0.0356	0.0762	0.0762	0.0356	0.0762	0.0762	0.0762	0.0762	0.0762	0.0762	0.0762	
Thickness, cm:	0.114	0.114	0.0458	0.0458	0.114	0.114	0.0458	0.114	0.114	0.114	0.114	0.114	0.114	0.114	
Minimum gage	0.122	0.122	0.0518	0.0518	0.122	0.122	0.0518	0.122	0.122	0.122	0.122	0.122	0.122	0.122	
Pressure load cylinder	0.0813	0.0813	0.0325	0.0325	0.0813	0.0813	0.0325	0.0813	0.0813	0.0813	0.0813	0.0813	0.0813	0.0813	
Design cylinder	0.089	0.089	0.0406	0.0406	0.089	0.089	0.0406	0.089	0.089	0.089	0.089	0.089	0.089	0.089	
Pressure load dome	32.8	32.8	40.1	40.1	32.8	32.8	40.1	32.8	32.8	32.8	32.8	32.8	32.8	32.8	
Design dome	6.8	6.8	8.2	8.2	41.5	41.5	61.2	45	45	45	45	45	45	45	
Mass, kg:	39.6	39.6	48.3	48.3	74.3	74.3	101.3	27.6	27.6	27.6	27.6	27.6	27.6	27.6	
Membrane															
Local strengthening															
Total															
Oxidizer tank:	2219-T81 Al	2219-T81 Al	Electro-formed Ni	Electro-formed Ni	2219-T81 Al	2219-T81 Al	Electro-formed Ni	2219-T81 Al	2219-T81 Al	2219-T81 Al	Electro-formed Ni	2219-T81 Al	2219-T81 Al	2219-T81 Al	
Material	2.8x10 ⁴	2.8x10 ⁴	6.9x10 ⁴	6.9x10 ⁴	2.8x10 ⁴	2.8x10 ⁴	6.9x10 ⁴	2.8x10 ⁴	2.8x10 ⁴	2.8x10 ⁴	6.9x10 ⁴	2.8x10 ⁴	2.8x10 ⁴	2.8x10 ⁴	
Working stress, N/cm ²	69	28	69	28	28	28	28	28	28	28	28	28	28	28	
Ullage pressure, N/cm ²	0.0762	0.0762	0.0356	0.0356	0.0762	0.0762	0.0356	0.0762	0.0762	0.0762	0.0356	0.0762	0.0762	0.0762	
Thickness, cm:	0.204	0.0813	0.0813	0.0813	0.0813	0.0813	0.0325	0.0813	0.0813	0.0813	0.0204	0.0813	0.0813	0.0813	
Minimum gage	0.211	0.089	0.0864	0.0864	0.089	0.089	0.0406	0.089	0.089	0.089	0.0406	0.089	0.089	0.089	
Pressure load	79.2	33.6	94.0	44.0	33.6	33.6	44.0	29.6	29.6	29.6	41.2	37.9	37.9	37.9	
Design	15.8	6.8	18.6	8.9	6.8	6.8	8.9	5.9	5.9	5.9	8.2	7.6	7.6	7.6	
Mass, kg:	95.0	40.4	112.6	52.9	40.4	40.4	52.9	35.5	35.5	35.5	49.4	45.5	45.5	45.5	
Membrane	70.8	31.8	70.8	31.8	31.8	31.8	31.8	31.8	31.8	31.8	31.8	31.8	31.8	31.8	
Local strengthening															
Total															
Helium tank:	Al and fiber glass	Al and fiber glass	Stainless steel and fiber glass	Stainless steel and fiber glass	Al and fiber glass	Al and fiber glass	Stainless steel and fiber glass	Al and fiber glass	Al and fiber glass	Al and fiber glass	Stainless steel, fiber glass, and Al	Al and fiber glass	Al and fiber glass	Al and fiber glass	
Material	60.0	60.0	58.0	58.0	60.0	60.0	58.0	60.0	60.0	60.0	113.0	137.0	137.0	137.0	
Mass, kg	265.4	171.8	289.7	289.7	171.8	171.8	289.7	206.5	206.5	206.5	245.8	245.8	245.8	245.8	
Total tankage and structure mass, kg															

The 69 N/cm² requirement of the nominal stage (column 1) provides sufficient margin for pressure increase due to propellant heating regardless of vehicle orientation. It also features state-of-the-art aluminum material. A reduction in the total tankage and structural mass of 93.6 kilograms could be achieved by lowering the flox tank pressure requirement to 28 N/cm² (column 2).

This comparison indicates the magnitude of the penalty associated with maintaining the flox pressure requirement at 69 N/cm². If the orientation is restricted to that of payload to the Sun, some reduction in flox tank pressure could be realized. However, a reduction to a 28 N/cm² level is improbable due to the problem of freezing the methane. Fabricating the tanks from stainless steel and electro-formed nickel (columns 3 and 4) yields slightly heavier total masses than aluminum tankage. It is therefore concluded that the tankage and structural mass is fairly insensitive to tank pressure and material selection. A detailed structural mass breakdown for the nominal stage is shown in table VI.

Three additional 6350-kilogram propellant load configurations were also designed for comparison with the nominal common bulkhead configuration. These configurations

TABLE VI. - TANKAGE AND STRUCTURAL MASS BREAKDOWN FOR THE 6350-KILOGRAM METHANE-FLOX COMMON BULKHEAD CONFIGURATION

[All masses are in kilograms.]

Tankage:		
Methane tank (Al) ^a	39.6	
Flox tank (Al) ^b	95.0	
Helium tank (Ti)	<u>70.8</u>	
Total		205.4
Structure:		
Payload adapter:		
Ring	7.3	
Struts (fiber glass)	7.3	
Struts fittings (16)	<u>5.4</u>	
Total	20.0	
Forward ring	25.5	
Aft ring	6.3	
Thrust cone	<u>8.2</u>	
Total		<u>60.0</u>
Total tankage and structure mass		265.4

^a28 N/cm².

^b69 N/cm².

were (1) a nested tank, (2) two separate tanks, and (3) four separate tanks. Design summaries for these configurations are also shown in table V.

The nested tank configuration is nearly identical in appearance to the nominal stage (fig. 13) except the methane tank would have a self-supporting reversed bulkhead. When columns 2 and 5 of table V are compared, it is evident that the nested tank configuration is heavier than the common bulkhead. Also, the fabrication of the reversed bulkhead is more difficult than that of the common bulkhead, while the thermal storage characteristics of the two configurations are about the same. It was therefore concluded that the common bulkhead configuration was preferable to the nested tank configuration.

The two-tank configuration (fig. 14) was analyzed because it removes the necessity of having a common liquid temperature (i. e., high oxidant tank pressure). This configuration offers a little mass advantage over the nominal stage; and, in certain cases,

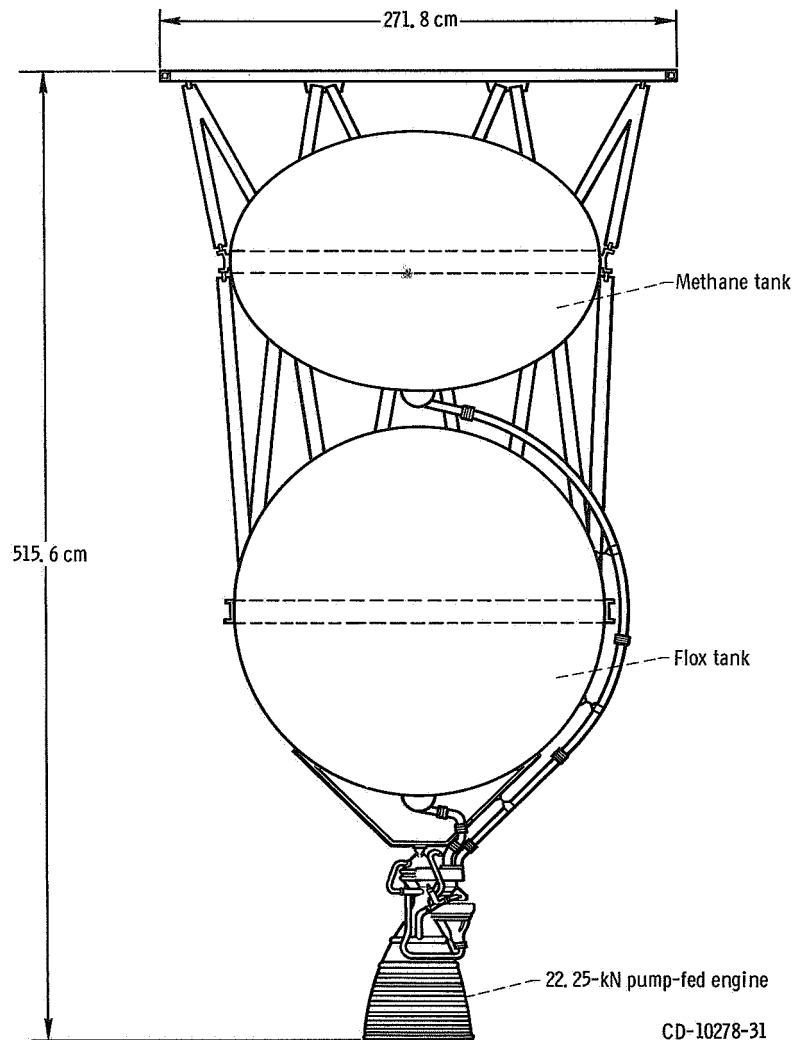


Figure 14. - Schematic of 6350-kilogram methane-flox two-tank retrostage.

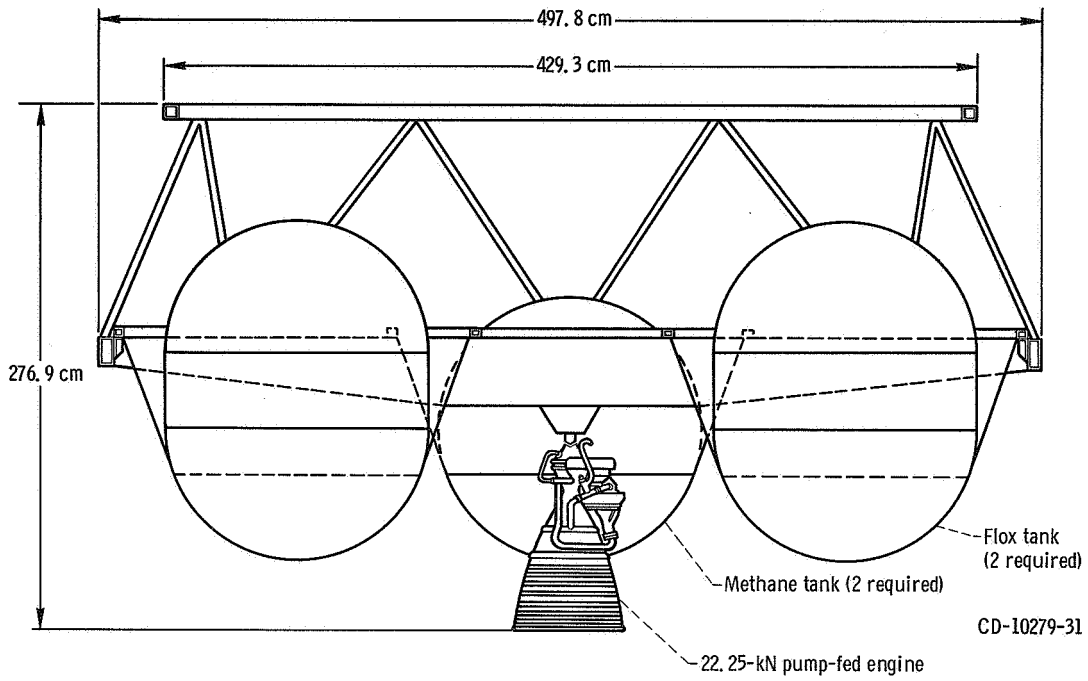


Figure 15. - Schematic of 6350-kilogram methane-flox four-tank retrostage.

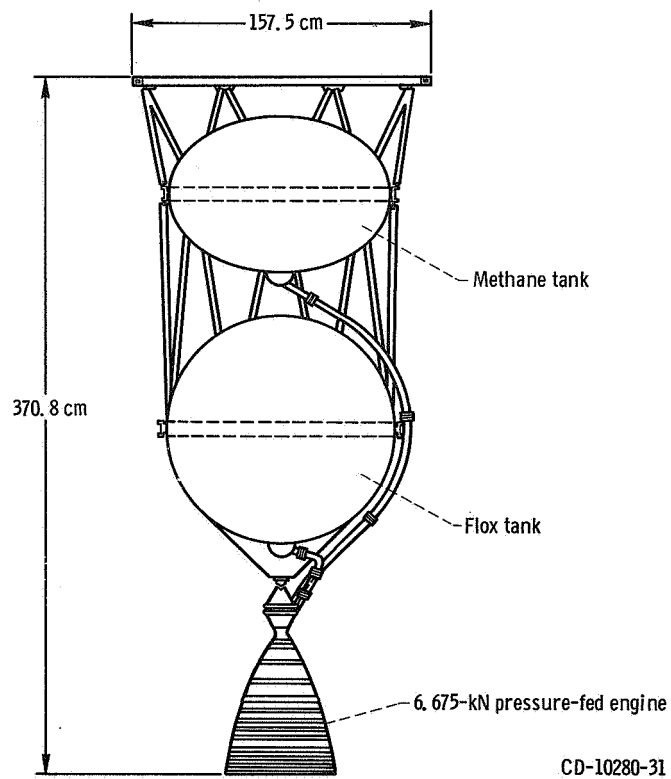


Figure 16. - Schematic of 1360-kilogram methane-flox two-tank retrostage.

it is more attractive when propellant heating is concerned. Therefore, this configuration was considered as a possible alternate stage.

The four-tank configuration (fig. 15) also negates the necessity of a high oxidant tank pressure and offers a very compact design. However, the mass of this stage is nearly twice that of the nominal. In addition, this configuration is very difficult to analyze thermally. Because of these considerations, this configuration was not considered further.

Two 1360-kilogram propellant load stages were designed using a two-tank configuration. The first utilized a pressure-fed engine (fig. 16) and the second a pump-fed engine. The pump-fed stage is identical in appearance to the pressure-fed stage except for the engine.

Again, 2219-T81 aluminum was selected as the tankage material and the structure utilized fiber glass struts as in the previous designs.

The tank design pressures were as follows:

Tank	Design pressure, N/cm ²	
	Pressure-fed stage	Pump-fed stage
Methane	110	28
Flox	138	69

TABLE VII. - TANKAGE AND STRUCTURAL MASS BREAKDOWN FOR THE 1360-KILOGRAM PRESSURE-FED, METHANE-FLOX TWO-TANK CONFIGURATION

[All masses are in kilograms.]

Tankage:

Methane tank (Al) ^a	20.0	
Flox tank (Al) ^b	23.0	
Helium tank (Ti)	<u>53.1</u>	
Total		96.1

Structure:

Payload adapter:		
Ring	4.5	
Struts (fiber glass)	5.0	
Strut fittings (16)	<u>5.4</u>	
Total		14.9
Methane tank ring		11.8
Main struts:		
Struts (fiber glass)	20.0	
Strut fittings	<u>6.3</u>	
Total		26.3
Flox tank ring		5.0
Thrust cone		<u>6.4</u>
Total		<u>64.4</u>

Total tankage and structure mass

160.5

^a110 N/cm².

^b138 N/cm².

TABLE VIII. - TANKAGE AND STRUCTURAL MASS BREAKDOWN

FOR THE 1360-KILOGRAM PUMP-FED, METHANE-FLOX

TWO-TANK CONFIGURATION

[All masses are in kilograms.]

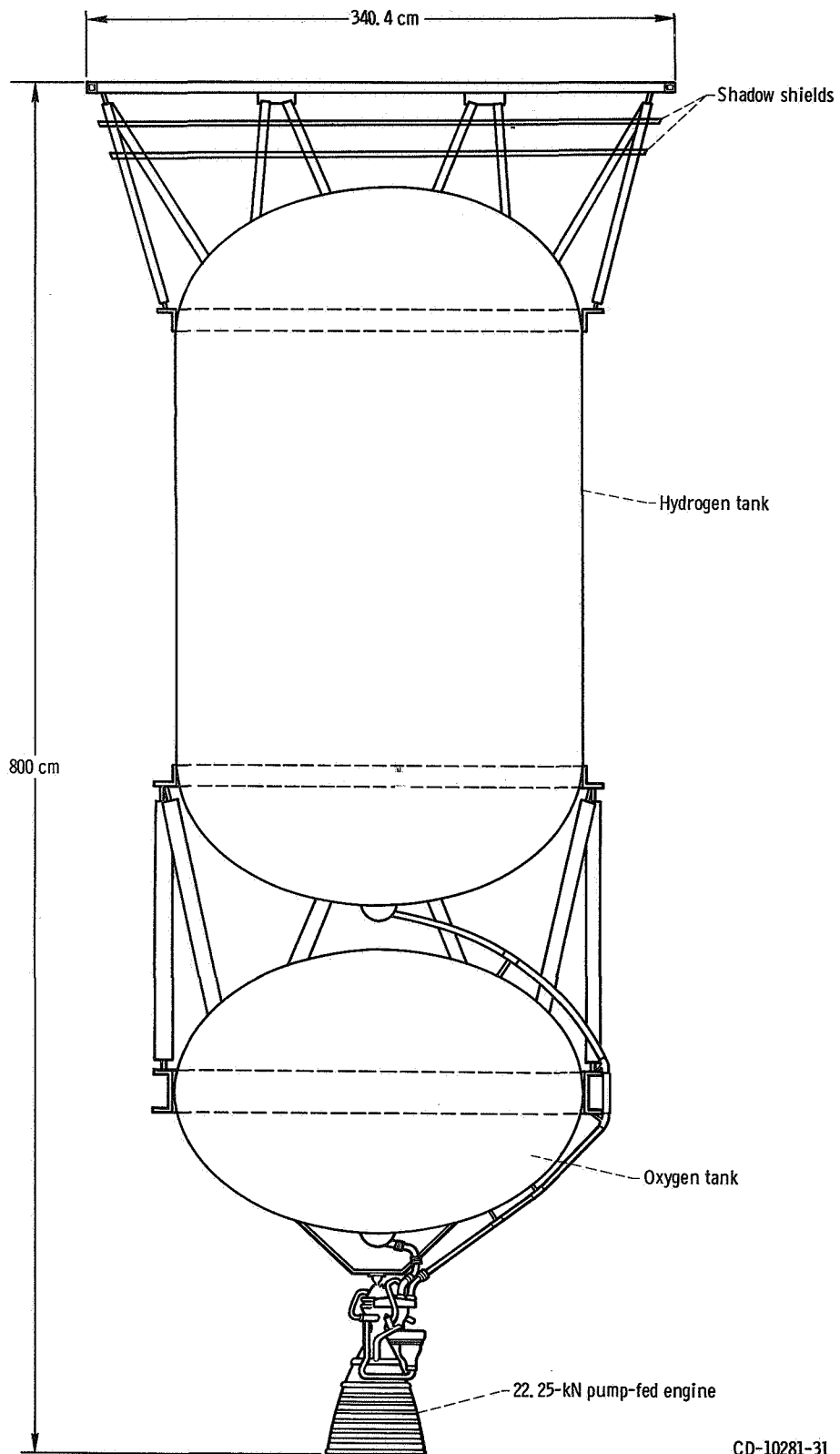
Tankage:		
Methane tank (Al) ^a	9.8	
Flox tank (Al) ^b	12.5	
Helium tank (Ti)	<u>7.3</u>	
Total		29.6
Structure:		
Payload adapter:		
Ring	4.5	
Struts (fiber glass)	5.0	
Strut fittings (16)	<u>5.4</u>	
Total		14.9
Methane tank ring		11.8
Main struts:		
Struts (fiber glass)	20.0	
Strut fittings	<u>6.3</u>	
Total		26.3
Flox tank ring		5.0
Thrust cone	<u>6.4</u>	
Total		<u>64.4</u>
Total tankage and structure mass		94.0
^a 28 N/cm ² .		
^b 69 N/cm ² .		

Detailed structural mass breakdowns are shown for the pressure- and pump-fed stages in tables VII and VIII, respectively.

Tankage was also sized for a 1360-kilogram common bulkhead configuration in order to conduct a thermal analysis comparison. However, no detailed design was included.

Hydrogen-Oxygen Propellant Combination

A 6350-kilogram propellant load hydrogen-oxygen stage was sized for performance comparison with the 6350-kilogram methane-flox stages. A simple two-tank configuration (fig. 17) was selected in an effort to minimize the heat flux to the hydrogen. The



CD-10281-31

Figure 17. - Schematic of 6350-kilogram hydrogen-oxygen retrostage.

TABLE IX. - DESIGN SUMMARY FOR THE 6350-KILOGRAM DEEP

CRYOGENIC AND EARTH STORABLE CONFIGURATIONS

	Configuration		
	Two-tank		Common bulkhead
	Propellant combination		
	Hydrogen-oxygen	Hydrogen-fluorine	Monomethyl hydrazine - mixed oxides of nitrogen (MMH-MON)
Fuel tank:			
Material	2219-T81 Al	2219-T81 Al	301-1/2 hard stainless steel
Working stress, N/cm ²	2.8×10 ⁴	2.8×10 ⁴	6.9×10 ⁴
Ullage pressure, N/cm ²	41	41	28
Thickness, cm:			
Minimum gage	0.0762	0.0762	0.0356
Pressure load cylinder	0.18	0.173	0.0432
Design cylinder	0.188	0.1805	0.0484
Pressure load dome	0.127	0.122	0.0305
Design dome	0.134	0.1295	0.0406
Mass, kg:			
Membrane	157.0	78.4	36.3
Local strengthening	31.3	15.9	7.3
Total	188.3	94.3	43.6
Oxidizer tank:			
Material	2219-T81 Al	2219-T81 Al	301-1/2 hard stainless steel
Working stress, N/cm ²	2.8×10 ⁴	2.8×10 ⁴	6.9×10 ⁴
Ullage pressure, N/cm ²	41	41	52
Thickness, cm:			
Minimum gage	0.0762	0.0762	0.0356
Pressure load	0.127	0.122	0.056
Design	0.134	0.1295	0.0635
Mass, kg:			
Membrane	56.1	48.6	55.8
Local strengthening	11.3	9.7	11.3
Total	67.4	58.3	67.1
Helium tank:			
Mass, kg (Tank pressure, 2.8×10 ³ N/cm ²)	54.4	41.0	28.1
Structure:			
Material	Al and fiber glass	Al and fiber glass	Al and stainless steel
Mass, kg	195.5	173.9	61.7
Total tankage and structure mass, kg	505.6	367.5	200.5

TABLE X. - TANKAGE AND STRUCTURAL MASS BREAKDOWN FOR THE 6350-
KILOGRAM HYDROGEN-OXYGEN CONFIGURATION

[All masses are in kilograms.]

Tankage:		
Hydrogen tank (Al) ^a	188.3	
Oxygen tank (Al) ^a	67.4	
Helium tank (Ti)	<u>54.4</u>	310.1
Total		
Structure:		
Payload adapter:		
Ring	9.5	
Struts (fiber glass)	20.4	
Strut fittings (16)	5.4	
Shadow shields	8.2	
Shield brackets (48)	<u>5.4</u>	
Total		48.9
Hydrogen tank forward ring	23.1	
Hydrogen tank aft ring	31.3	
Main struts:		
Struts (fiber glass)	45.4	
Strut fittings	<u>7.3</u>	
Total		52.7
Oxygen tank ring	31.3	
Thrust cone	<u>8.2</u>	
Total		<u>195.5</u>
Total tankage and structure mass		505.6

^a41 N/m².

space truss assembly utilized fiber glass struts to reduce the conductive heat transfer

Again, 2219-T81 aluminum was selected for the tankage and the tank diameter was fixed by the oblate spheroid oxygen tank. The tank design ullage pressure was 41 N/cm² for both tanks.

A design summary is shown in table IX while a detailed mass breakdown is given in table X.

Hydrogen-Fluorine Propellant Combination

A 6350-kilogram propellant load hydrogen-fluorine stage was also sized for per-

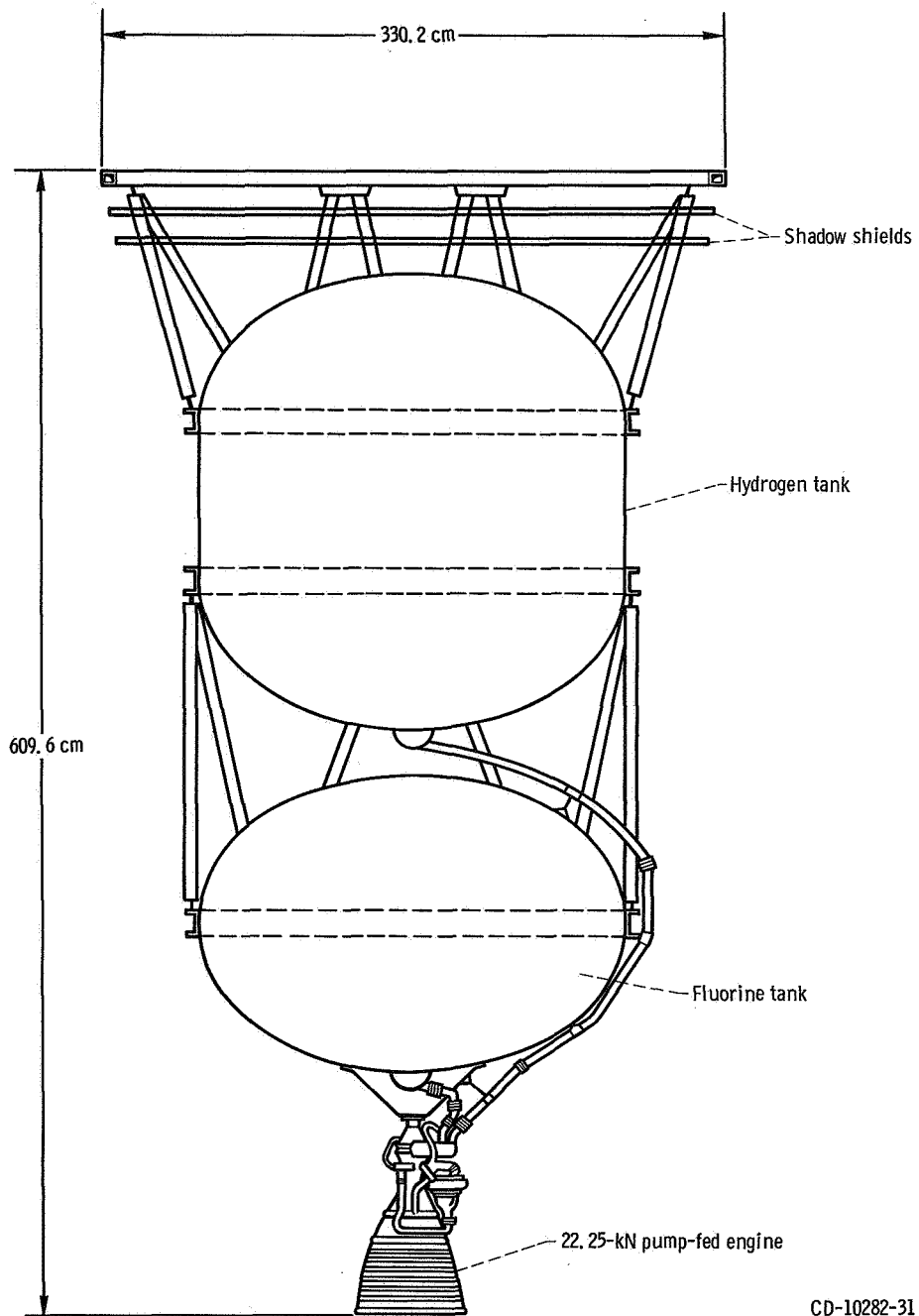


Figure 18. - Schematic of 6350-kilogram hydrogen-fluorine retrostage.

formance comparison with the 6350-kilogram methane-flox stages. A simple two-tank configuration (fig. 18) similar to the hydrogen-oxygen configuration was selected. The hydrogen-fluorine stage design approach, materials, tank pressure, and general description are identical to the hydrogen-oxygen stage. The design summary for the hydrogen-fluorine stage is also shown in table IX while a detailed mass breakdown is given in table XI.

TABLE XI. -TANKAGE AND STRUCTURAL BREAKDOWN FOR THE 6350-KILOGRAM HYDROGEN-FLUORINE CONFIGURATION

[All masses are in kilograms.]

Tankage:		
Hydrogen tank (Al) ^a	94.3	
Fluorine tank (Al) ^a	58.3	
Helium tank (Ti)	<u>41.0</u>	
Total		193.6
Structure:		
Payload adapter:		
Ring	8.2	
Struts (fiber glass)	18.6	
Strut fittings (16)	5.4	
Shadow shields	8.2	
Shield brackets (48)	<u>5.4</u>	
Total		45.8
Hydrogen tank forward ring	21.8	
Hydrogen tank aft ring	29.5	
Main struts:		
Struts (fiber glass)	31.8	
Strut fittings	<u>7.3</u>	
Total		39.1
Fluorine tank ring	29.5	
Thrust cone	<u>8.2</u>	
Total		<u>173.9</u>
Total tankage and structure mass		367.5
^a 41 N/cm ² .		

Earth Storable Propellant Combinations

For the Earth storable propellants, both a 6350-kilogram propellant load pump-fed stage and a 1360-kilogram propellant load pressure-fed stage were evaluated. For these stages, the ullage volumes were reduced to 5 percent because propellant heating was not a problem.

The pump-fed stage design was based on a common bulkhead configuration (fig. 19). The propellant tanks and thrust structure were designed for 301-1/2 hard stainless steel

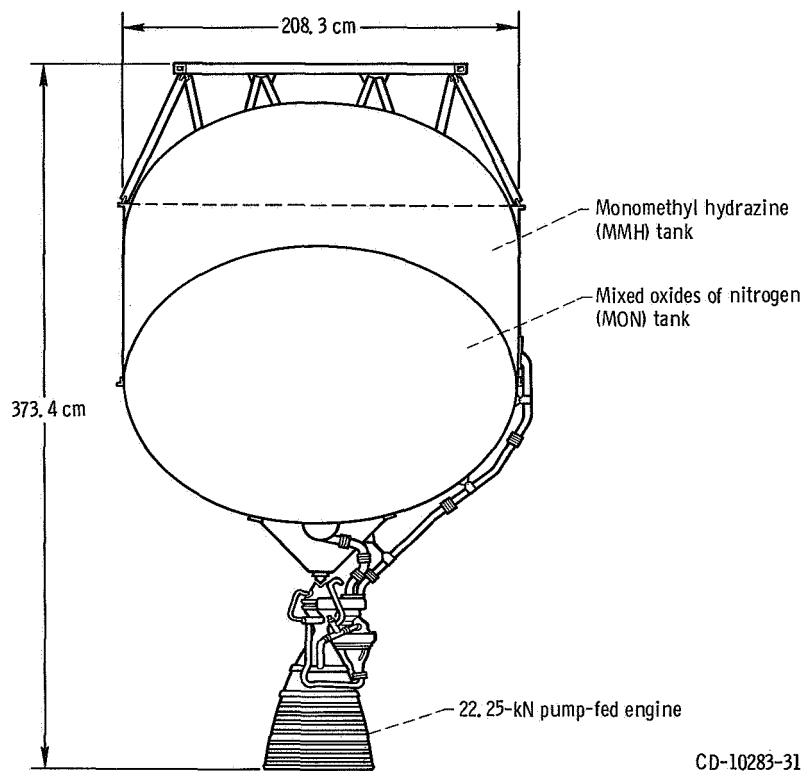


Figure 19. - Schematic of 6350-kilogram Earth storable common bulkhead retrostage.

which, for this configuration, yields a lighter system weight than aluminum. Since conduction from the payload is not a problem with these propellants, the use of aluminum (2219-T81) was assumed for the payload adapter.

The design summary for the 6350-kilogram stage is also shown in table IX while a detailed mass breakdown is presented in table XII.

Although a common bulkhead configuration similar to the previous stage would be somewhat lighter, the 1360-kilogram pressure-fed stage was designed using a two-tank configuration (fig. 20) so that a direct performance comparison could be made with the 1360-kilogram methane-flox stages.

TABLE XII. - TANKAGE AND STRUCTURAL MASS BREAKDOWN FOR THE 6350-
KILOGRAM EARTH STORABLE COMMON BULKHEAD CONFIGURATION

[All masses are in kilograms.]

Tankage:		
MMH tank (stainless steel) ^a	43.6	
MON tank (stainless steel) ^b	67.1	
Helium tank (Ti)	<u>28.1</u>	
Total		138.8
Structure:		
Payload adapter:		
Ring	7.3	
Struts (Al)	5.4	
Strut fittings (16)	<u>4.5</u>	
Total		17.2
Forward ring	21.3	
After ring	13.2	
Thrust cone	<u>10.0</u>	
Total		<u>61.7</u>
Total tankage and structure mass		200.5

^a28 N/cm².
^b52 N/cm².

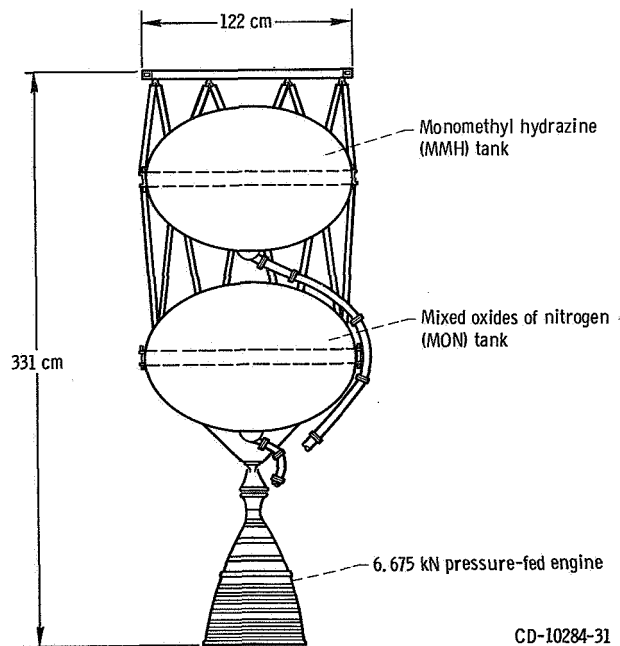


Figure 20. - Schematic of 1360-kilogram Earth storable two-tank retrostage.

TABLE XIII. - TANKAGE AND STRUCTURAL MASS BREAKDOWN FOR THE 1360-KILOGRAM PRESSURE-FED, EARTH STORABLE TWO-TANK CONFIGURATION

[All masses are in kilograms.]

Tankage:		
MMH tank (Al) ^a	21.3	
MON tank (Al) ^b	29.0	
Helium tank (Ti)	<u>28.1</u>	
Total		78.4
Structure:		
Payload adapter:		
Ring	6.8	
Struts (Al)	4.5	
Strut fittings (16)	<u>5.4</u>	
Total		16.7
MMH tank ring	10.9	
Main struts:		
Struts (Al)	18.1	
Strut fittings	<u>6.4</u>	
Total		24.5
MON tank ring	10.4	
Thrust cone	<u>6.4</u>	
Total		<u>68.9</u>
Total tankage and structure mass		147.3

^a110 N/cm².

^b138 N/cm².

Aluminum (2219-T81) was selected for the propellant tanks and tank support rings. Stainless steel tanks would be lighter than the aluminum tanks, but adding stainless steel support rings to get weld compatibility results in an overall assembly mass greater than that with aluminum. The fuel and oxidant tanks were designed for 110 and 138 N/cm², respectively. A detailed mass breakdown for this stage is shown in table XIII.

THERMAL CONTROL

Introduction and Assumptions

The primary uncertainty in determining the nonvented space storability of a given

propellant combination is the distribution of the heat entering the propellant tanks. If the net heat transfer is into the tanks and the liquid is uniformly heated, then the allowable space storage time can be (depending on the magnitude of the heat flux and the maximum allowable tank pressure) several orders of magnitude longer than if a substantial amount of the heat entering the tanks goes into vaporizing liquid. If, however, the net heat transfer is out of the tanks, then the problem becomes one of propellant freezing rather than overpressurizing the tanks.

The approach taken in this study was that of assuming 100 percent bulk heating in the cases where the net heat was into the tanks with provision being made to prevent freezing of the propellants when the net heat was out of the tanks. That is, all heat entering or leaving the tanks uniformly heats or cools the liquid, respectively.

It may be necessary to provide some active thermal conditioning system (e.g., a mixer) to obtain complete bulk heating; however, at relatively low heat fluxes such as were encountered in this study, heat-transfer calculations based on a pure conduction model tend to agree with those based on a bulk heating model (ref. 5).

When selecting a thermal protection system for long duration missions requiring storage of cryogenic propellants, the choice of multilayer insulation or a combination of multilayer and another insulation (e.g., foam) is inevitable because of the superior performance of the multilayer over other insulations.

However, additional methods of reducing the heat transfer are available in conjunction with using multilayer insulation. These methods are as follows:

- (1) Jettisoning the shroud surrounding the propellant tanks after launch through the atmosphere so that the propellants can radiate to the cold environment of space
- (2) Separating the warm and cold propellant tanks as far apart as reasonable and also placing the payload as far from the propellant tank as reasonable to reduce the radiation heat transfer to the propellants
- (3) Utilizing shadow shields; that is, discretely spaced thermal radiation barriers between the heat source and heat sink to further reduce the radiation heat transfer
- (4) Selecting a low-conductivity support system to substantially reduce the heat transfer by conduction (e.g., fiber glass instead of aluminum)

The assumptions used in the thermal analysis were the following:

- (1) Tanks were insulated with multilayer insulation having a density of 0.08 gram per cubic centimeter. References 6 to 12 provide substantial information on the performance and properties of multilayer insulation systems which show the latitude available in selecting materials that can be used as components of a multilayer insulation system. The insulation weights quoted in tables II and III are consistent with a system containing double-aluminized mylar radiation shields and dexiglass spacers. Comparable insulation weights could be attained by selecting other materials.

(2) Stages were not exposed to direct aerodynamic heating. The payload and upper stage were shrouded during launch. After launch through the atmosphere, the shroud was jettisoned and the tanks were free to radiate to space.

(3) The initial methane and flox temperature was 100 K in the common bulkhead stages. In the two-tank stages, the initial methane temperature was 111 K and the flox was 88.9 K.

(4) The initial temperature of the hydrogen was 20.6 K and that of the oxygen and fluorine was 88.9 K.

(5) Initial Earth storable temperatures were 288.9 K. The propellant vapor pressures (i. e., initial tank pressures) corresponding to the previous initial temperatures are given in table XIV.

(6) The payload was represented by a disk equal to the stage diameter and kept at 294.4 K.

(7) In the methane-flox and Earth storable stages, the payload was one-quarter the tank radius above the tank; in the hydrogen-oxygen and hydrogen-fluorine stages, it was one-half the tank radius above the tank. These distances were not optimized in this study, but preliminary calculations indicated them to be reasonable for stages of these sizes.

(8) For the nominal cases, a multilayer insulation having a 3.81-centimeter thickness was selected with the emissivity and thermal absorptivity of surfaces not receiving

TABLE XIV. - INITIAL TANK PRESSURES
OF PROPELLANTS

Propellant	Initial temperature, K	Initial tank pressure, N/cm ²
Methane	100	3.45
	111	9.65
Flox (82.5 percent fluorine/17.5 percent oxygen) ^a	100	36.5
	88.9	14.7
Hydrogen	20.6	11.0
Fluorine	88.9	14.7
Oxygen	88.9	20.0
Monomethyl hydrazine (MMH)	288.9	.41
Mixed oxides of nitrogen (MON)	288.9	48.3

^aVapor pressure of fluorine was used as the flox vapor pressure for conservatism.

solar radiation being 0.1. In the orientations where some surfaces received solar radiation, the solar absorptivity was 0.3 and the emissivity was 0.9 on these surfaces. These values correspond to the properties of an existing white paint known to be relatively insensitive to ultraviolet radiations (refs. 13 and 14).

(9) No boost heating analysis was included, but the stages were assumed to be vented during boost; or, alternatively, it was assumed that the propellants could be subcooled before launch to allow for the absorption of heat during boost.

(10) The only heat sources considered during the coast were solar and onboard.

(11) Based on the results in the mission analysis section, the coast times to Saturn were 1100 and 1500 days for the 6350- and 1360-kilogram propellant loadings, respectively. Similarly, the coast times to Jupiter were 500 and 600 days.

Due to the uncertainty in the actual thermal performance of multilayer insulation on space vehicle tanks, a conservative nominal thickness of 3.81 centimeters was selected. As mentioned previously, various investigations have been conducted to determine the effective conductivity of multilayer insulations, and the results indicate values both higher and lower than those reported in reference 11. However, most of the information has been obtained on relatively small samples and thicknesses. In a current in-house Lewis test program, data are being generated on a large liquid hydrogen tank utilizing a multilayer insulation system. Preliminary results seem to indicate thermal conductivities around 1.7×10^{-4} watt per meter per degrees Kelvin (W/m K) for hot and cold insulation boundary temperatures of 275 and 20.6 K. These experimental data points on the large tank are about 10 times greater than the best values obtained on small samples and are about a factor of 5 greater than that predicted in reference 11. Data have also been generated on a large liquid hydrogen tank utilizing a different multilayer insulation system in reference 15. These data indicate a thermal conductivity of 3×10^{-5} W/m K with boundary temperatures of 125 and 20.6 K which is about a factor of 2 greater than that predicted in reference 11. Thus, in order to allow for a degradation of predicted insulation conductivity on large tanks, the thickness of 3.81 centimeters was selected as the nominal with the thermal conductivity quoted in reference 11 multiplied by a factor of 2. The effects of further increases in thermal conductivity will be shown subsequently.

As far as surface properties are concerned, emissivity data have been generated on multilayer insulation radiation shields. In the temperature range involved, the data indicate emissivities of the order of 0.01 (ref. 16). Based on the data presented in reference 8, it does not appear that aluminized surfaces are severely damaged by contamination due to high humidity, high temperature, carbon dioxide, or salt environments for periods up to 100 hours. Therefore, the surface properties should remain stable. However, since uncertainties still exist, we assumed that the nominal emissivity and thermal absorptivity of surfaces not "seeing" the Sun was 0.10. The effects of having a lower and a higher value than nominal will also be shown subsequently.

The modes of heat transfer considered in this study were (1) radiation interchange between the payload and the fuel tank, (2) conduction through support members neglecting thermal contact resistance, (3) radiation interchange between propellants in the two tank stages, and (4) radiation to space from surfaces which are not influenced by any other heat source.

Methane-Flox Stages

For the methane-flox stages, it was found that for either engine to the Sun or payload to the Sun orientation, conduction heat transfer through the truss structure into the propellants could be eliminated through proper selection of the truss tube material and external emissivity. This is illustrated in figure 21 for the 6350-kilogram common bulk-head configuration. This figure shows support external emissivity plotted against support thermal conductivity for zero conduction into or out of the propellant tank. As can be seen from the curve, with fiber glass struts an emissivity of only 0.02 is required to maintain zero conduction. For titanium or stainless steel struts, the required emissivities are 0.25 and 0.54, respectively. Any combination of thermal conductivity and emissivity that lies below the curve would result in propellant heating, and any combination falling above the curve would produce propellant cooling. Due to the latitude available in se-

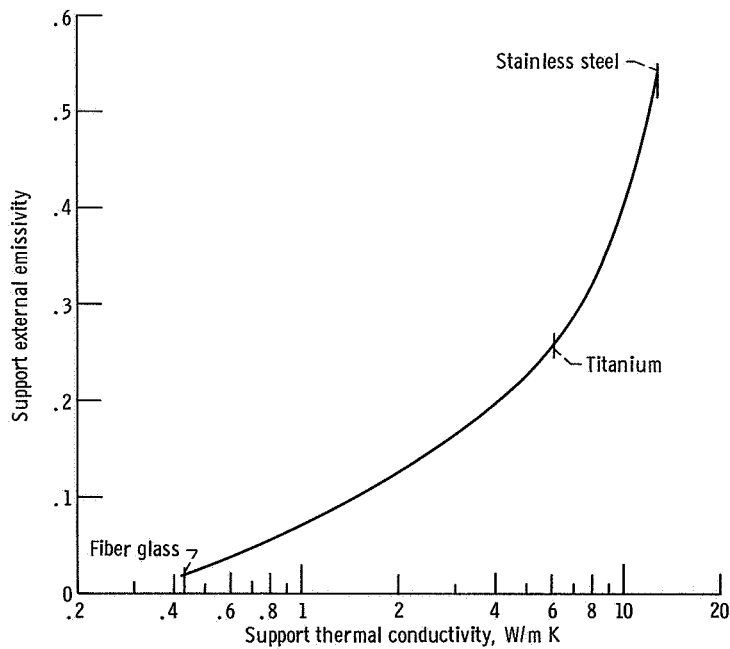


Figure 21. - Support external emissivity plotted against thermal conductivity; zero conduction heat transfer. 6350-Kilogram methane-flox common bulk-head configuration; payload temperature, 294.4 K; tank temperature, 100 K.

lecting support material and surface coating to maintain zero conduction, this mode of heat transfer was considered zero for the methane-flox stages for these orientations.

With velocity vector orientation, calculations assuming solar heating on the bare struts results in excessive heat transfer to the propellant. Therefore, in this orientation, the struts were assumed to be insulated with multilayer insulation to eliminate the effect of solar heating on the conduction heat transfer.

As mentioned previously, radiation between propellant tanks was considered in the two-tank configurations. Results of the analyses show that even though one tank "sees" the other, the view factor between the tanks and the difference in storage temperatures considered are so low that neither tank is significantly affected by the presence of the other. Therefore, it was assumed that the entire flox tank and the bottom of the methane tank radiated to the cold environment of space in these configurations.

It was also found that the methane-flox stages required no shadow shields between the payload and methane tank except for velocity vector oriented cases where one shield was used to eliminate the heat transfer from the payload.

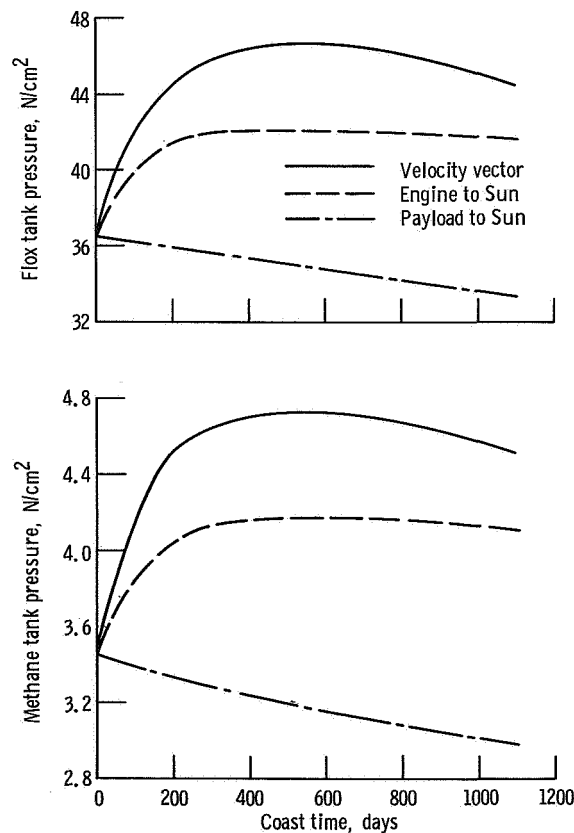


Figure 22. - Tank pressures plotted against coast time for three stage orientations. Nominal thermal performance; 6350-kilogram methane-flox common bulkhead configuration.

The effects of stage orientation and size are shown in figures 22 to 24. Figures 22 and 23 are for 1100-day Saturn missions using 6350-kilogram configurations. From a space heating point of view, the early part of the trajectory is similar to a 500-day Jupiter trajectory. Therefore, tank pressure data for both the Saturn and Jupiter missions on the larger stages can be read from these curves using the proper trip times. Figure 22 shows tank pressures as a function of time for the 6350-kilogram common bulkhead configuration with nominal insulation performance and surface properties for three different orientations. The maximum tank pressure occurs in the velocity vector orientation, but its value in the flox tank is less than 48 N/cm^2 , which is well below the design value of 69 N/cm^2 . The methane tank pressure exhibits the same characteristic but is an order of magnitude lower. It should also be noted that in both the engine to the Sun oriented and velocity vector oriented cases, the tank pressure initially rises and then decays while the payload to Sun orientation constantly decays.

Figure 23 shows similar data for the 6350-kilogram two-tank configuration. This figure exhibits the same trend as figure 22, but the flox tank pressure rise in the engine to the Sun orientation shows less variation than the common bulkhead while the payload to Sun orientation shows a greater variation. No velocity vector oriented curve is shown

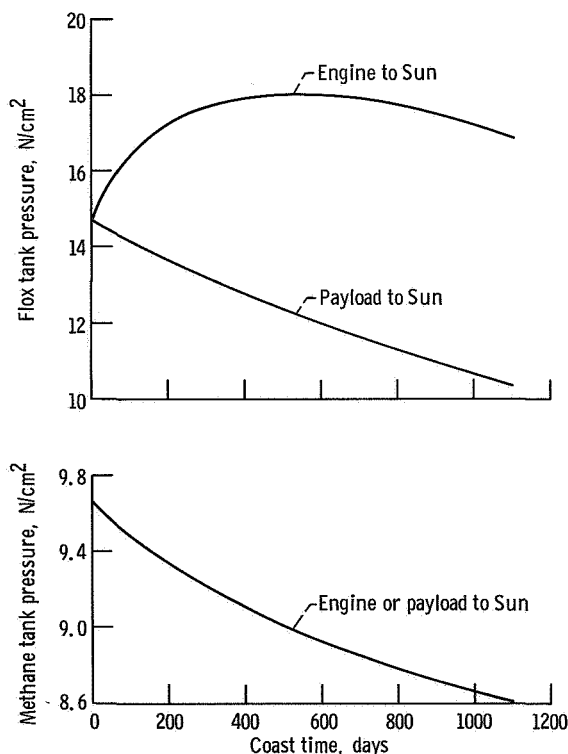


Figure 23. - Tank pressures plotted against coast time for two stage orientations. Nominal thermal performance; 6350-kilogram methane-flox two-tank configuration.

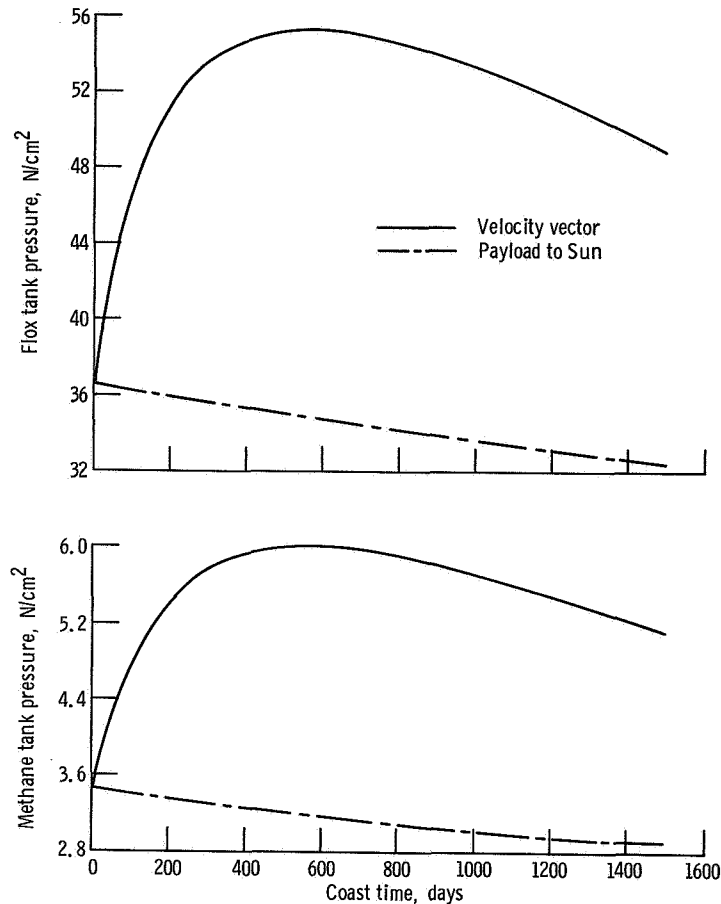


Figure 24. - Tank pressures plotted against coast time for two stage orientations. Nominal thermal performance; 1360-kilogram methane-flox common bulkhead configuration.

on the figure because of the difficulty in analyzing the reflections between the tanks in this configuration, but the pressure variation would be less than in the common bulkhead configuration.

Figure 24 shows similar data for a 1500-day Saturn mission using the 1360-kilogram common bulkhead configuration. The early part of this trajectory approximates a 600-day Jupiter trajectory and data for missions to both planets on the smaller stages can again be read from the same curves. This figure shows that the pressure rise in the velocity vector orientation is somewhat greater than the 6350-kilogram case while the decrease in pressure in the payload to Sun orientation is about the same. However, the results do not change significantly with propellant loading.

The effects of thermal property degradation on the stages in a payload to Sun orientation are shown in figures 25 to 28. The primary concern is the uncertainty in the actual performance of the installed multilayer insulation with less concern for the stability of the surface properties of the surfaces. Surface coatings are affected by the

ultraviolet radiation from the Sun, while metallized surfaces appear much less affected. However, since in the payload to Sun orientation, none of the surfaces "see" the Sun, the surface properties should remain stable.

Figure 25 shows the effect of insulation effectiveness and external surface emissivity on final tank pressure for the 6350-kilogram common bulkhead configuration. The nominal performance point on this and the following figures is at 100 percent effectiveness and 0.10 emissivity.

Insulation effectiveness as used herein can be viewed as percent of the reciprocal of nominal insulation thermal conductivity or as percent of the nominal insulation thickness. First, if one assumes the insulation thickness to remain constant at the nominal value of 3.81 centimeters, then insulation effectiveness is inversely proportional to insulation thermal conductivity. One hundred percent corresponds to nominal conductivity, 50 percent corresponds to twice nominal conductivity, etc. On the other hand, if one assumes that the effective thermal conductivity remains constant at the nominal value, then insulation effectiveness is proportional to insulation thickness. One hundred percent corresponds to 3.81 centimeters; 50 percent corresponds to 1.905 centimeters, etc. The ensuing discussion concentrates on the percent of the nominal insulation thermal conductivity approach.

For this and the following figures, it was assumed that the deviation from the nominal existed for the entire mission time. If the deviation varied as a function of time, the associated performance penalty would decrease. It should be noted that the emissivities

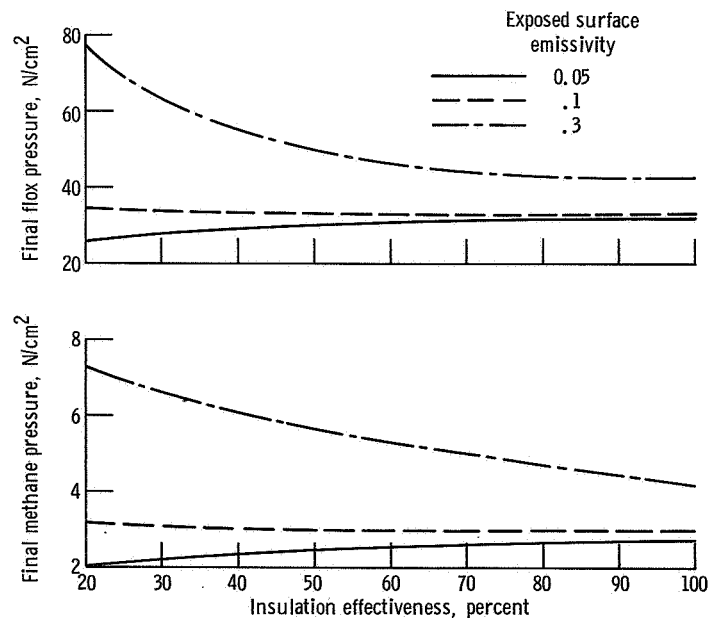


Figure 25. - Final tank pressures plotted against insulation effectiveness for 6350-kilogram methane-flox common bulkhead configuration. Payload to Sun orientation; coast time, 1100 days.

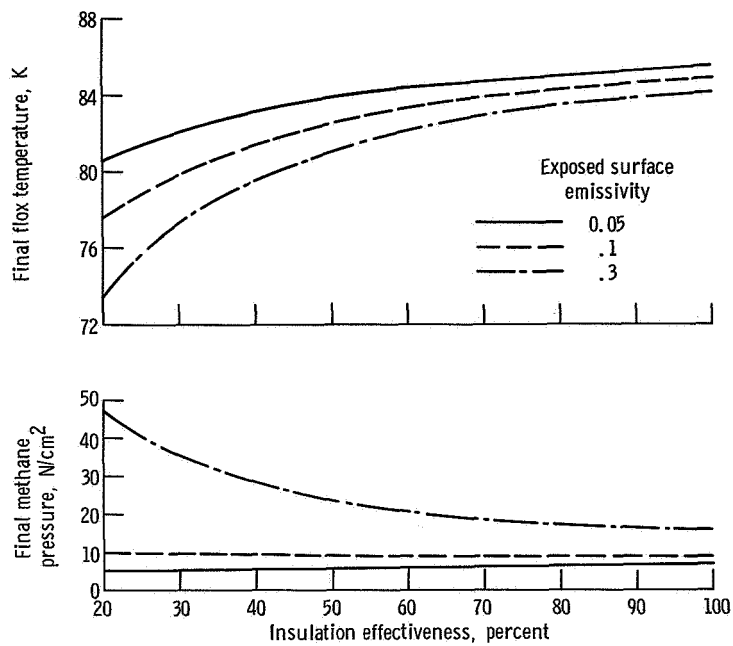


Figure 26. - Final flux temperature and final methane pressure plotted against insulation effectiveness for 6350-kilogram methane-flox two-tank configuration. Payload to Sun orientation; coast time, 1100 days.

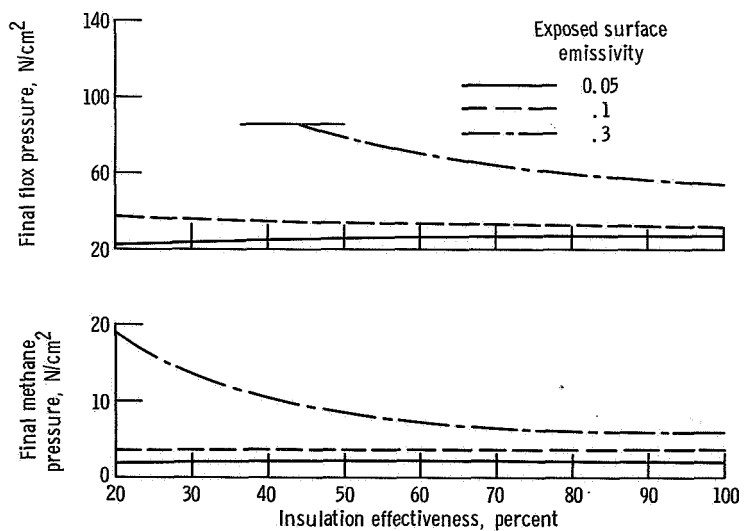


Figure 27. - Final tank pressures plotted against insulation effectiveness for 1360-kilogram methane-flox common bulkhead configuration. Payload to Sun orientation; coast time, 1500 days.

shown refer to all exposed surfaces; and, if one surface changes by a certain amount, they all change by the same amount which is a very conservative assumption. The only surface of the multilayer insulation considered to be affected was the outermost layer. The figure shows that the configuration can tolerate substantial variations in both emissivity and insulation performance without exceeding tank pressure limits.

Similar data are shown for the 6350-kilogram two-tank configuration in figure 26. Although the methane tank pressure is an order of magnitude higher than the common bulkhead configuration due to the higher initial temperature, the trends are the same. Flox temperature is plotted in this figure instead of pressure as in the previous figures because when the tanks are separated, the flox temperature and/or pressure continually decreases. When this occurs, the concern is that of freezing the flox. As can be seen, the final flox temperature is relatively insensitive to insulation and optical property variation. Since the flox freezing point is around 52.8 K, the danger of freezing is small.

Figure 27 shows the results for the 1360-kilogram common bulkhead configuration. The results are comparable to those in figure 25 for low emissivity surfaces; however, the pressure rise is much greater for the combination of high emissivities and poor insulation performance. The horizontal line denoting the left terminus of the high emissivity curve for the flox tank indicates that the expanding liquid has occupied the total tank volume (i. e., ullage = 0). Increasing the initial ullage volume would allow further degradation of the thermal properties at the expense of system weight.

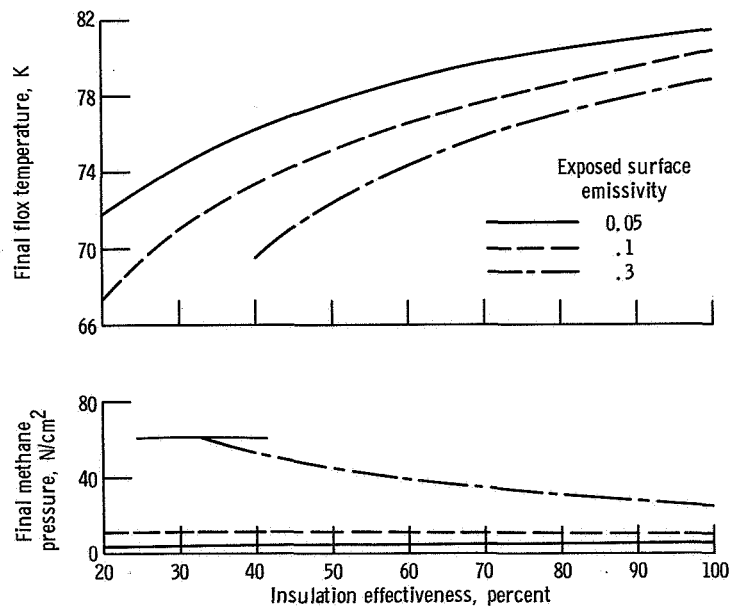


Figure 28. - Final flox temperature and final methane pressure plotted against insulation effectiveness for 1360-kilogram methane-flox two-tank configuration. Payload to Sun orientation; coast time, 1500 days.

The results for the 1360-kilogram two-tank configuration are shown in figure 28. This figure exhibits the same trend as figure 26; however, the pressure rise in the methane tank is greater at a combination of high emissivity and poor insulation performance and the floc temperature lower and closer to the freezing point.

Hydrogen-Oxygen and Hydrogen-Fluorine Stages

The thermal analysis in these stages was restricted to a 6350-kilogram propellant loading and a payload to Sun orientation. Unlike the methane-floc stages, the conduction heat transfer to the hydrogen could not be eliminated due to the much lower fuel temperature. Even with fiber glass supports having an external emissivity of 1.0, heat would be conducted into the hydrogen tank. Therefore, this mode of heat transfer was included in the analysis.

Also unlike the methane-floc, the radiation exchange between the tanks was somewhat different. Instead of both tanks effectively seeing space, the hydrogen tank was affected by the oxygen and fluorine tanks; but the oxidant tanks were not affected by the hydrogen tank. Calculations show that the net heat transfer to the hydrogen, however, was very close to zero and sometimes slightly negative depending on the oxidant temperature. Therefore, it was assumed that the net heat to the hydrogen by radiation from the oxidant tanks was zero and the oxidant tanks radiated to a zero degree environment.

Two shadow shields were equally spaced between the payload and the hydrogen tank in these stages. Shadow shields are discretely spaced thermal radiation barriers placed between a heat source and heat sink in order to allow some of the radiant energy from the heat source to be reradiated to the cold environment of space and thus effectively reduce the heat transfer to the heat sink (see fig. 17). Analytical investigations of the effectiveness of shadow shields of various shapes (i. e., flat plates, spheres, cones, etc., and combinations thereof) have been reported in references 17 to 22. An experimental program was conducted to determine the actual effectiveness of multiple flat shields and the results are presented in reference 23. Multilayer insulation was used on the forward and aft bulkheads of the hydrogen tanks and on the oxidant tanks. In addition, 1.27 centimeters of foam insulation, for ground hold purposes, was placed on the cylindrical section and under the multilayer insulation on the bulkheads of the hydrogen tank. Utilizing a high emissivity surface (0.9) permitted a significant increase in the heat rejection rate from the tank sidewalls. The fiber glass supports were assumed to have an emissivity of 0.8.

Figure 29 shows oxygen tank temperature and hydrogen tank pressure as functions of coast time for the nominal thermal properties (i. e., 3.81 cm of multilayer insulation and emissivities of 0.1). As in the methane-floc two-tank configurations, the oxidant

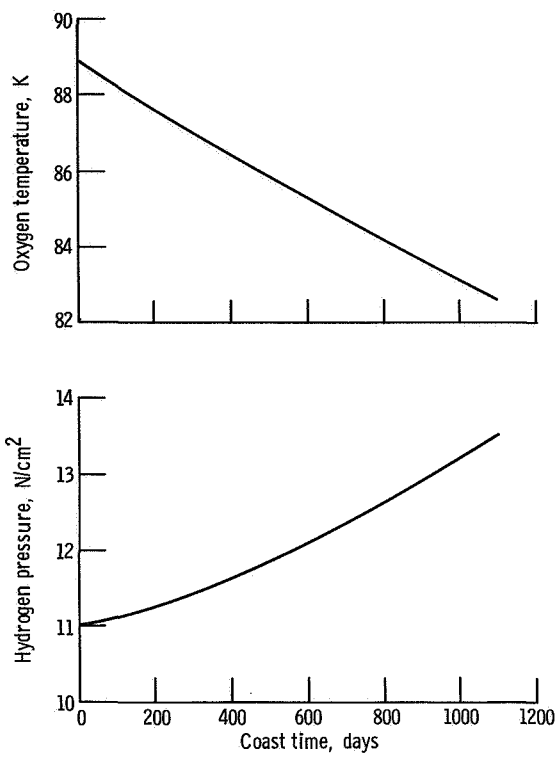


Figure 29. - Oxygen temperature and hydrogen pressure plotted against coast time for 6350-kilogram stage. Nominal thermal performance.

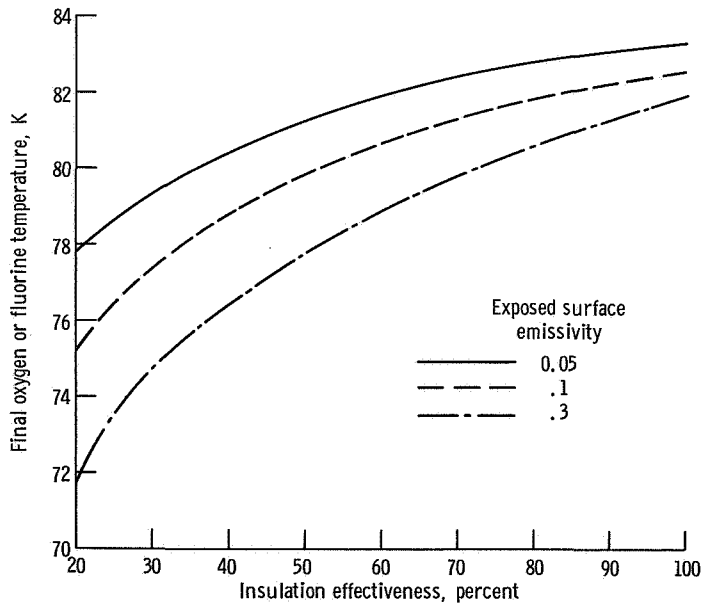


Figure 30. - Final oxidizer temperature plotted against insulation effectiveness for 6350-kilogram hydrogen-oxygen and hydrogen-fluorine stages. Payload to Sun orientation; coast time, 1100 days.

temperature decreases with time. However, its final value is well above the freezing point of oxygen. The hydrogen pressure increases, but the pressure rise is only about 2.5 N/cm^2 over 1100 days.

Figure 30 shows the final oxygen or fluorine temperature as a function of insulation and surface property degradation. The results are also similar to the flox tank in the 6350-kilogram two-tank configuration discussed previously.

Figure 31 shows the effect of insulation and surface property degradation on the final hydrogen tank pressure for the hydrogen-fluorine stage. This figure shows that

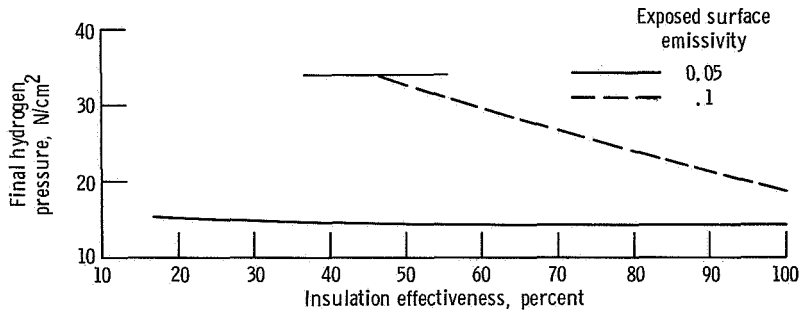


Figure 31. - Final hydrogen pressure plotted against insulation effectiveness for 6350-kilogram hydrogen-fluorine stage. Payload to Sun orientation; coast time, 1100 days.

the hydrogen tank pressure is very sensitive to insulation effectiveness even with the nominal emissivity, but relatively insensitive to insulation performance if the emissivities are below the nominal. Again, the emissivities shown refer to all exposed surfaces; and, if one surface changes by a certain amount, they all change by the same amount. However, this does not apply to the cylindrical section or support emissivities whose assumed values were mentioned previously (i. e., 0.9 and 0.8, respectively). As in the methane-flox stages, the only surface of the multilayer insulation which was considered affected was the outermost layer.

Figure 32 presents similar results for the hydrogen-oxygen stage. The hydrogen tank pressure is less sensitive to degradation than in the hydrogen-fluorine stage because of the lower O/F ratio. This increases the mass of the hydrogen, thus increasing the heat sink capability. It also increases the hydrogen tank cylindrical section surface area which allows more heat to be radiated to space.

In the previous discussion, only foam insulation was placed on the cylindrical section of the hydrogen tank. This aided in rejecting heat when the tank did not have solar or planetary radiation incident on it. However, during the early portion of the mission, an Earth orbital coast period may be desirable where having only foam on the cylindrical section may cause excessive heat transfer to the tank.

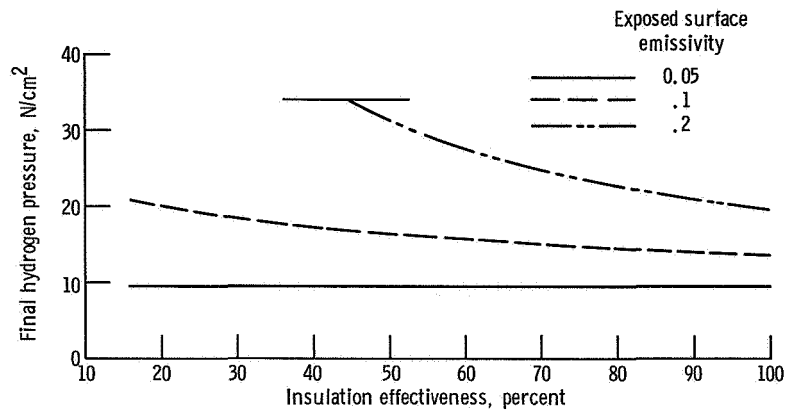


Figure 32. - Final hydrogen pressure plotted against insulation effectiveness for 6350-kilogram hydrogen-oxygen stage. Payload to Sun orientation; coast time, 1100 days.

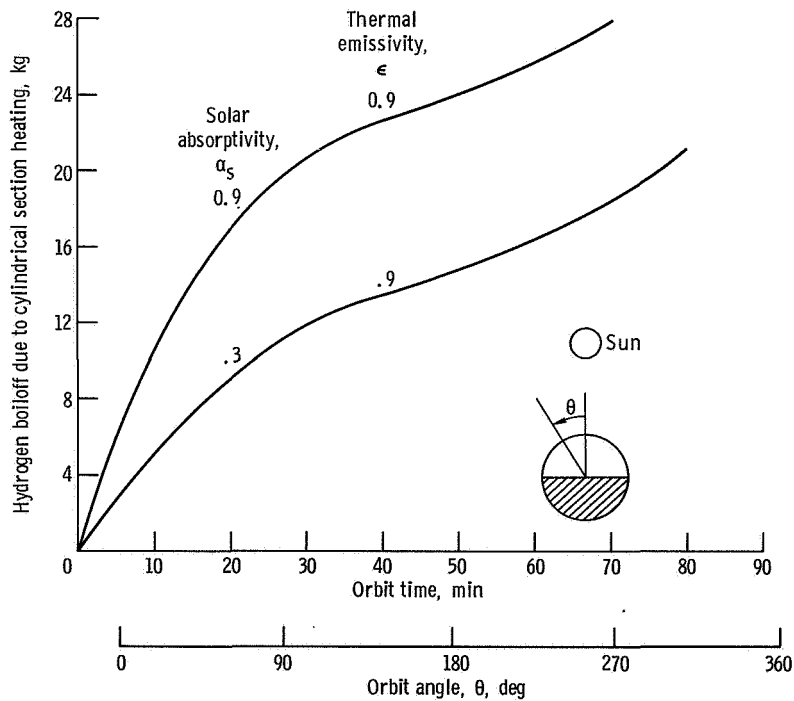


Figure 33. - Hydrogen boiloff plotted against time in orbit for 6350-kilogram hydrogen-oxygen stage. Hydrogen cylindrical section; 1.27 centimeters of foam insulation; 90-nautical-mile circular orbit; velocity vector oriented; complete stratification model.

In a parking orbit environment, the heat flux to a vehicle is considerably higher than that encountered during an interplanetary coast. With this high heat flux, the assumption of bulk heating is questionable. Therefore, an estimate of the heat flux to the cylindrical section of the hydrogen tank in the hydrogen-oxygen stage was made assuming (1) all heat that entered the tank boiled off liquid, and (2) all heat that entered the tank went into bulk heating of the liquid. The heating rates as a function of orbit time and/or orbit travel angle measured from insertion were generated assuming a typical eastward launch into a 90 nautical mile circular orbit of low inclination. Insertion was assumed to occur at 10 a. m. The amount of hydrogen boiloff as a function of time spent in orbit, assuming all heat entering the tank boils off liquid, is shown in figure 33. Results are presented for two different foam insulation surface coatings.

The upper curve on this and the next figure shows the results when the foam has been painted black to yield a high solar absorptivity (α_s) and a thermal emissivity (ϵ) of 0.9. This approximates a worst case condition while a more realistic coating is shown by the lower curve. Boiloff depends on time in orbit and on the time of day at which coasting occurs. The curves can be used for any coast time or time of day by reading the boiloff at the angle corresponding to insertion and subtracting this value from the boiloff observed t minutes later, where t equals the coast time of interest. Figure 34

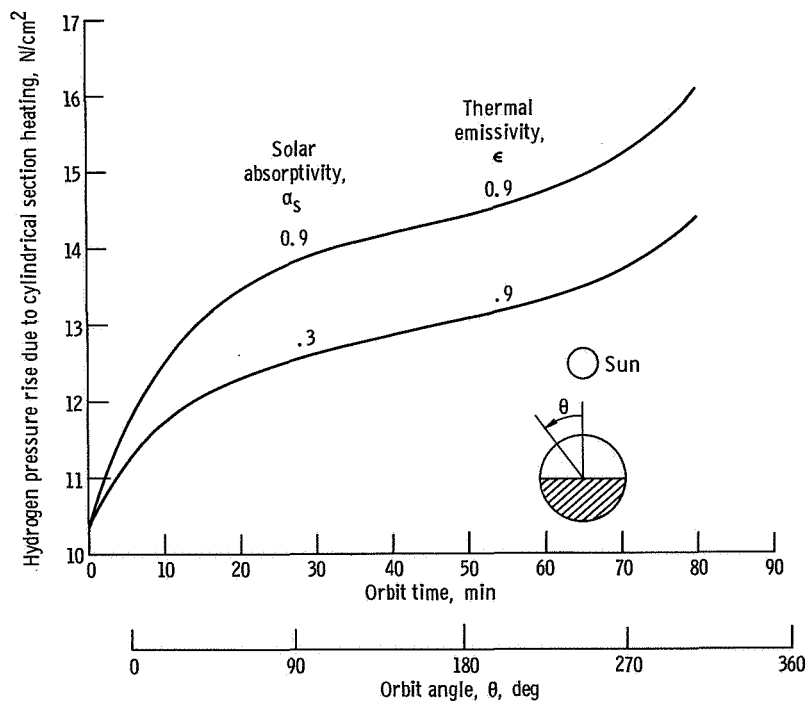


Figure 34. - Hydrogen pressure rise plotted against time in orbit for 6350-kilogram hydrogen-oxygen stage. Hydrogen cylindrical section; 1.27 centimeters of foam insulation; 90-nautical-mile circular orbit; velocity vector oriented; complete mixing model.

is similar to figure 33 except hydrogen tank pressure is plotted and the assumption of 100 percent bulk heating (with no resultant hydrogen boiloff) is used instead of 100 percent boiloff. As mentioned previously, by using mixers, a high degree of bulk heating can be maintained. Without mixers, the real case will probably lie in between these two extremes (i. e. , some vaporization and some bulk heating); however, the actual condition is unknown.

Earth Storable Stages

A thermal analysis was conducted for a 6350-kilogram common bulkhead configuration and a 1360-kilogram two-tank configuration. In each case, the tanks were assumed to be radiating to a 0° environment and receiving no heat from any source in order to see if propellant freezing occurred. Only the nominal performance is presented (i. e. , 3.81-cm multilayer insulation with an outer layer emissivity of 0.1).

The results are presented in figure 35. The solid curve shows temperature profiles plotted against coast time for the 6350-kilogram common bulkhead configuration. For

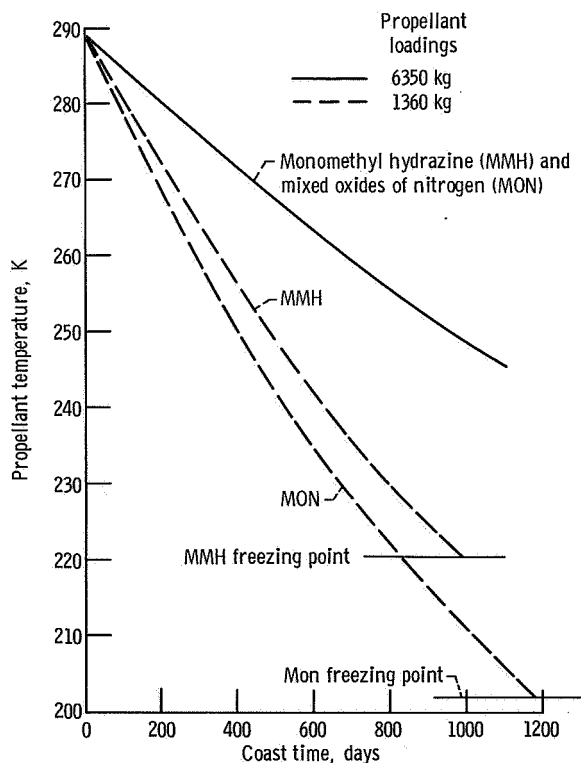


Figure 35. - Propellant temperatures plotted against coast time for two Earth storable propellant loadings. Nominal thermal performance; no incident heat.

nominal performance, neither propellant freezes over a period of 1100 days. The dashed curves show the results for the 1360-kilogram two-tank configuration. The total mission time again is 1500 days instead of 1100. The MMH freezes after 1000 days while the MON freezes after 1180 days.

It should be noted that this is the most severe condition for the Earth storable propellants. To alleviate the problems of degradation in thermal performance, the propulsion system could be integrated with the payload to substantially reduce the rate of heat loss.

Even for the completely isolated case considered previously, the power requirement to prevent freezing is quite small - of the order of 1 watt per tank. This would appear to be a small additional burden on the power supply when one considers that spacecraft power requirements of 100 watts or more are not unlikely for planetary orbit missions.

MISSION PERFORMANCE

In this section, the performance of the various retrostages will be compared using the values of specific impulse and stage mass fraction established in the previous sections. The performance of the retrostages will be compared on a general basis first. They will then be compared specifically for the Jupiter and Saturn orbiter missions.

A general comparison between the performance of the various large (6350-kilogram propellant weight) retrostages is shown in figure 36. Payload fraction is shown as a

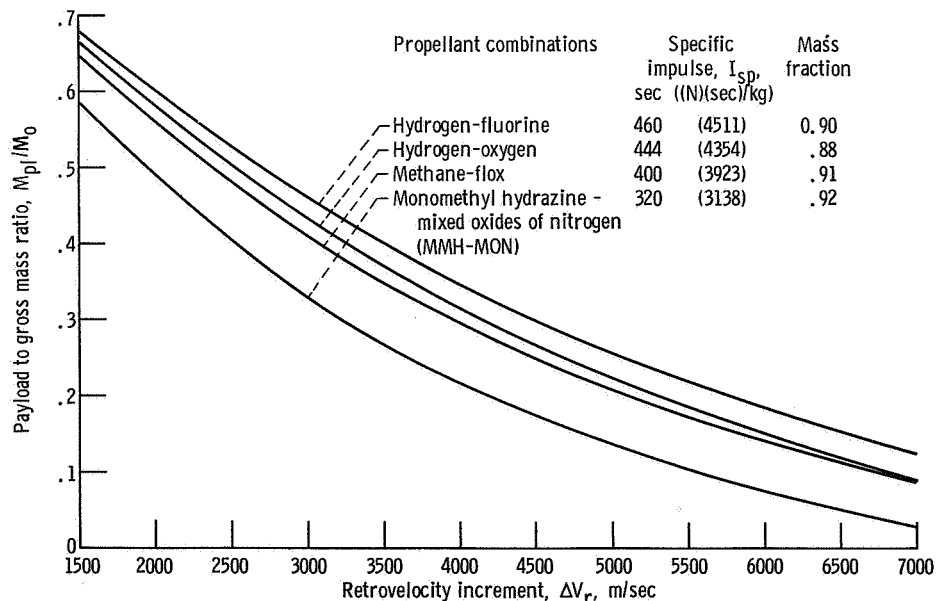


Figure 36. - Payload to gross mass ratio as function of retrovelocity increment for several pump-fed propellant combinations. Propellant mass, 6350 kilograms.

function of stage characteristic velocity (ΔV). The payload fraction shown is the ratio of payload mass (M_{PL}) to total stage gross mass (M_0) including payload. The figure indicates that, from a performance standpoint, the higher mass fractions which are possible with the Earth storable and space storable propellants cannot overcome the advantage in specific impulse held by the deep cryogenics.

A similar comparison for the small planetary retrostages (1360-kg propellant load) is shown in figure 37. The performance of both pump- and pressure-fed methane-flox stages are compared to the performance of a pressure-fed Earth storable stage. The deep cryogenic stages were not investigated for the small stage size.

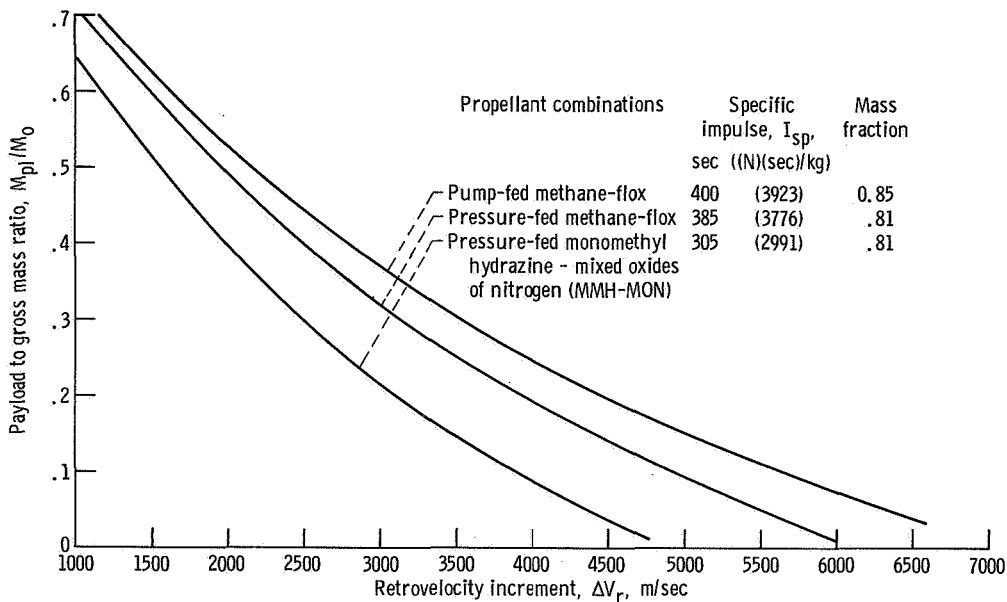


Figure 37. - Payload to gross mass ratio as function of retrovelocity increment for several propellant combinations. Propellant mass, 1360 kilograms.

The performance of the various planetary retrostages for Jupiter and Saturn orbiter missions is summarized in figures 38 to 41. Figure 38 presents results for a Jupiter orbiter mission using the 260-inch solid launch vehicle. The trade-off between apoapsis radius and trip time is presented for each of the small retrostages delivering a final payload of 907 kilograms. A constant periapsis radius of 3.0 planet radii is assumed. It should again be noted that for all retrostages it was assumed that the electrical, tracking, and telemetry systems and all guidance and attitude control functions were integrated with the payload. Thus, the 907-kilogram payload must provide for these systems.

As shown in figure 38, a Jupiter orbiter mission can be accomplished with a 260-inch solid launch vehicle and a pressurized Earth storable retromodule. As an ex-

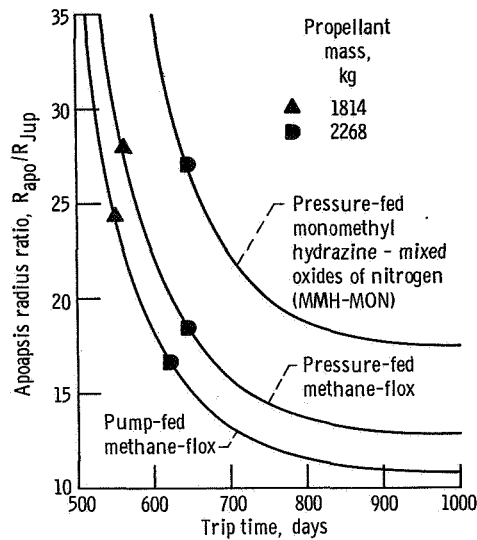


Figure 38. - Apoapsis radius ratio plotted against trip time to Jupiter for various propellant combinations. Periapsis radius ratio, R_{peri}/R_{Jup} , 3.0; 260-inch solid/S-IV B/Centaur; payload, 907 kilograms.

ample, the 907-kilogram payload can be delivered to an orbit having a periapsis radius of 3.0 planet radii and an apoapsis radius of 26.5 Jupiter radii in about 650 days. Use of the pump-fed methane-flox retrostage can reduce trip time about 110 days or decrease the apoapsis radius to about 15.0 Jupiter radii.

A payload comparison between the various retrostages can also be made using several of the figures mentioned previously. Again, consider the 650-day mission for the pressurized Earth storable stage. Figure 8 indicates that the 260-inch solid vehicle injects 3720 kilograms for this trip time. With a payload weight of 907 kilograms, the payload fraction for the pressurized Earth storable is 0.244. Reference to figure 37 shows that at this payload fraction, the pressure-fed Earth storable stage has a ΔV_r capability of 2825 meters per second and the corresponding payload fraction for the pump-fed methane-flox stage is 0.397. With this payload fraction and an injection mass of 3720 kilograms, the payload for the pump-fed methane-flox stage is approximately 1477 kilograms. For the same mission then (650-day trip time, a periapsis radius of 3.0 Jupiter radii, and an apoapsis radius of about 26.5 Jupiter radii), the 907-kilogram payload for the pressurized Earth storable stage can be increased to 1477 kilograms using a pump-fed methane-flox stage. Similar comparisons can be made for other points in figure 38.

It should be mentioned that the performance results shown in figure 38 are all based on the stage mass fractions obtained for the 1360-kilogram propellant mass designs. In

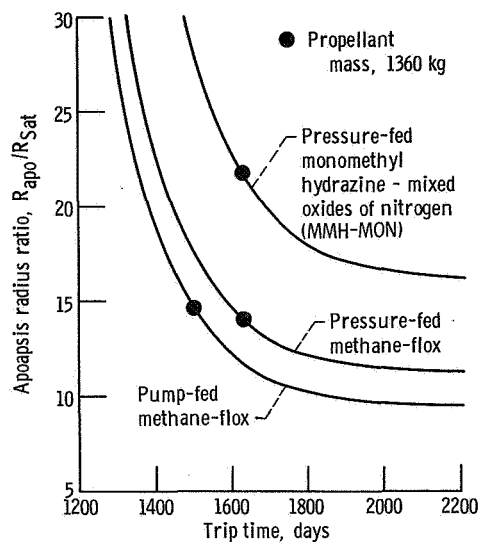


Figure 39. - Apoapsis radius ratio plotted against trip time to Saturn for various propellant combinations. Periapsis radius ratio, R_{peri}/R_{Sat} , 3.0; 260-inch solid/S-IV B/Centaur; payload, 907 kilograms.

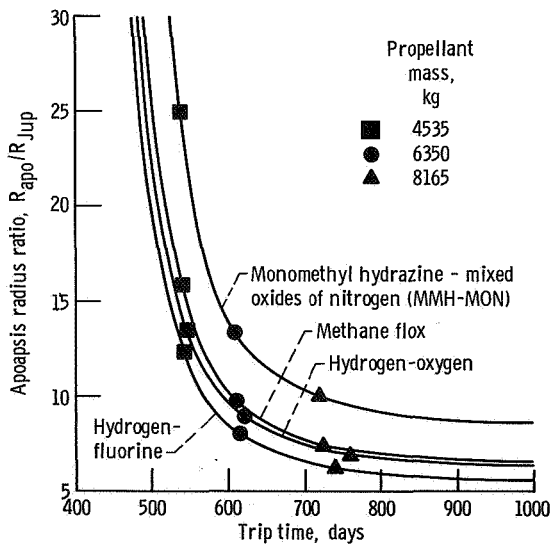


Figure 40. - Apoapsis radius ratio plotted against trip time to Jupiter for various propellant combinations. Periapsis radius ratio, R_{peri}/R_{Jup} , 3.0; Saturn V; payload, 1360 kilograms.

actually, the stage propellant loadings vary along the curves presented in figure 38. Several values of required stage propellant loading are indicated by the symbols on the figure. For stage propellant loadings higher than the design value of 1360 kilograms (as is the case throughout fig. 38), the stage mass fractions should presumably be somewhat better than the values used in the calculations. Similarly, where propellant loadings are smaller than the design value (as is the case in some of the following figures), the stage mass fraction should be somewhat lower than the values used in the calculations.

A comparison of the smaller retrostages for a Saturn orbiter mission using a 260-inch solid vehicle is shown in figure 39. Except for the longer trip times required, the results are similar to those for figure 38.

A comparison of the performance of the larger retrostages is shown in figures 40 and 41. Figure 40 gives results for a Jupiter orbiter mission using a Saturn V launch vehicle, and figure 41 gives results for a Saturn orbiter mission using a Saturn V/Centaur launch vehicle. The final payload for these larger missions has been increased to 1360 kilograms. (Significantly higher payloads could be assumed, if desired, at, of course, some sacrifice in either trip time, orbit radius, or both.) All the stages shown in figures 40 and 41 are pump-fed, and results for both hydrogen-oxygen and hydrogen-fluorine stages have been included.

The general trends and comparisons shown in figures 40 and 41 are similar to those presented in figures 38 and 39. With the larger launch vehicles, the orbiter missions can be accomplished in a shorter trip time or with closer planetary orbits or both.

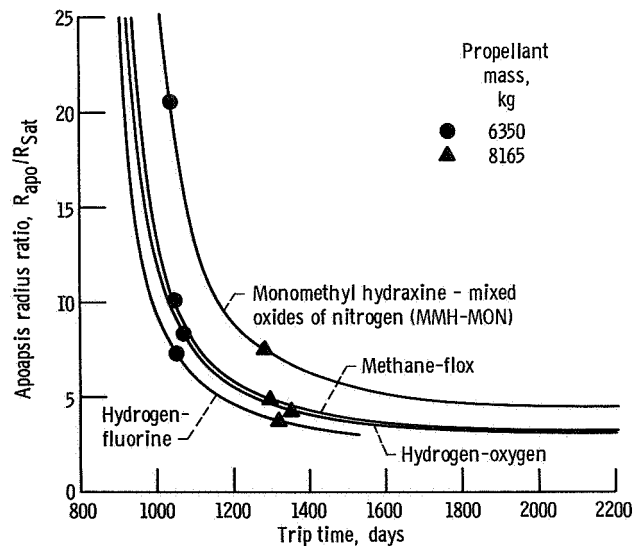


Figure 41. - Apoapsis radius ratio plotted against trip time to Saturn for various propellant combinations. Periapsis radius ratio, R_{peri}/R_{Sat} , 3.0; Saturn V/Centaur; payload, 1360 kilograms.

However, truly short trips or close circular orbits cannot be achieved even using Saturn V class launch vehicles.

SUMMARY OF RESULTS

An analytical study of unmanned planetary orbiter missions to Jupiter and Saturn was conducted in order to compare the payload capability and propellant storage characteristics of retrostages using Earth storable, space storable, and deep cryogenic propellants. The results may be summarized as follows:

1. Space storable stages utilizing multilayer insulation and low conductivity supports appear capable of remaining nonvented in space for long periods of time.

2. Utilizing payload to the Sun orientation plus shadow shields results in storability characteristics for the deep cryogenics that are similar to those of the space storables.

3. Space storable or deep cryogenic stages offer a payload advantage over Earth storable stages when compared on a fixed stage velocity increment basis. However, regardless of the propellant combination selected, the payload level can be significantly influenced by changes in trip-time, periapsis altitude, and orbit eccentricity. Therefore, the absolute advantage of the more energetic propellant combinations over Earth storables is largely determined by how rigidly the payload planner constrains the mission parameters.

Lewis Research Center,
National Aeronautics and Space Administration,
Cleveland, Ohio, January 15, 1969,
128-06-04-02-22.

REFERENCES

1. Anon.: The Meteoroid Satellite Project Pegasus First Summary Report. NASA TN D-3505, 1966.
2. Frost, V. C.: Aerospace Meteoroid Environment and Penetration Criterion. Rep. TOR-269 (4560-40)-2, Aerospace Corp., Aug. 17, 1964. (Available from DDC as AD-465431.)
3. Schmidt, Harold W.: Handling and Use of Fluorine and Fluorine-Oxygen Mixtures in Rocket Systems. NASA SP-3037, 1967.
4. Advanced Propulsion Staff: Fluorine Systems Handbook. Rep. DAC-59074, Douglas Aircraft Co. (NASA CR-72064), 1967.

5. Dowty, E. L.: Theoretical Pressure Histories for Cryogenic Fuel Tanks. Progress in Astronautics and Aeronautics. Vol. 20. G. B. Heller, ed., Academic Press, Inc., 1967, pp. 833-848.
6. Anon.: Liquid Propellant Losses During Spaceflight. Rep. ADL-65008-00-04, Arthur D. Little, Inc., Oct. 1963.
7. Black, Igor A.: Basic Investigation of Multi-Layer Insulation Systems. Rep. ADL-65958-00-04, Arthur D. Little, Inc. (NASA CR-54191), Oct. 30, 1964.
8. Anon.: Advanced Studies on Multi-Layer Insulation Systems. Rep. ADL-67180-00-04, Arthur D. Little, Inc. (NASA CR-54929), June 1, 1966.
9. Coston, R. M.: Handbook of Thermal Design Data for Multilayer Insulation Systems. Vol. II. Rep. LMSC-A847882, vol. 2, Lockheed Missiles and Space Co. (NASA CR-87485), June 25, 1967.
10. Sterbentz, W. H.; and Baxter, J. W.: Thermal Protection System for a Cryogenic Spacecraft Propulsion Module. Vol. II. Rep. LMSC-A794993, vol. 2, Lockheed Missiles and Space Co. (NASA CR-54879, vol. 2), Nov. 15, 1966.
11. Lindquist, C. R.: Super Insulation Applied to Space Vehicles. Linde Co., Dec. 1, 1962.
12. Glaser, Peter E.; Black, Igor A.; Lindstrom, Richard S.; Ruccia, Frank E.; and Wechsler, Alfred E.: Thermal Insulation Systems - A Survey. NASA SP-5027, 1967.
13. Schafer, Charles F.; and Bannister, Tommy C.: Thermal Control Coating Degradation Data from the Pegasus Experiment Packages. Progress in Astronautics and Aeronautics. Vol. 20. G. B. Heller, ed., Academic Press, Inc., 1967, pp. 457-473.
14. Plunkett, Jerry D.: NASA Contributions to the Technology of Inorganic Coatings. NASA SP-5014, 1964.
15. Anon.: Propellant Selection for Spacecraft Propulsion Systems. Vol. 3: Thermodynamics and Propulsion. Rep. LMSC-K-19-68-6, vol. 3, Lockheed Missiles and Space Co. (NASA CR-96740), Aug. 30, 1968.
16. Caren, R. P.: Low-Temperature Emittance Determinations. Progress in Astronautics and Aeronautics. Vol. 18. G. B. Heller, ed., Academic Press, Inc., 1966, pp. 61-73.
17. Smolak, George R.; Knoll, Richard H.; and Wallner, Lewis E.: Analysis of Thermal-Protection Systems for Space-Vehicle Cryogenic-Propellant Tanks. NASA TR R-130., 1962.

18. Jones, L. R. ; and Barry, D. G. : Lightweight Inflatable Shadow Shields for Cryogenic Space Vehicles. *J. Spacecraft Rockets*, vol. 3, no. 5, May 1966, pp. 722-728.
19. Nichols, Lester D. : Effect of Shield Position and Absorptivity on Temperature Distribution of a Body Shielded from Solar Radiation in Space. NASA TN D-578, 1961.
20. Nothwang, George J. ; Arveson, John C. ; and Hamaker, Frank M. : Analysis of Solar-Radiation Shields for Temperature Control of Space Vehicles Subjected to Large Changes in Solar Energy. NASA TN D-1209, 1962.
21. Arveson, John C. ; and Hamaker, Frank M. : Effectiveness of Radiation Shields for Thermal Control of Vehicles on the Sunlit Side of the Moon. NASA TN D-2130, 1964.
22. Boyle, Robert J. ; and Knoll, Richard H. : Thermal Analysis of Shadow Shields and Structural Members in a Vacuum. NASA TN D-4876, 1968.
23. Knoll, Richard H. ; and Bartoo, Edward R. : Experimental Studies on Shadow Shields for Thermal Protection of Cryogenic Tanks in Space. NASA TN D-4887, 1968.

POSTMASTER: If Undeliverable (Section 158
Postal Manual) Do Not Return

"The aeronautical and space activities of the United States shall be conducted so as to contribute . . . to the expansion of human knowledge of phenomena in the atmosphere and space. The Administration shall provide for the widest practicable and appropriate dissemination of information concerning its activities and the results thereof."

—NATIONAL AERONAUTICS AND SPACE ACT OF 1958

NASA SCIENTIFIC AND TECHNICAL PUBLICATIONS

TECHNICAL REPORTS: Scientific and technical information considered important, complete, and a lasting contribution to existing knowledge.

TECHNICAL NOTES: Information less broad in scope but nevertheless of importance as a contribution to existing knowledge.

TECHNICAL MEMORANDUMS: Information receiving limited distribution because of preliminary data, security classification, or other reasons.

CONTRACTOR REPORTS: Scientific and technical information generated under a NASA contract or grant and considered an important contribution to existing knowledge.

TECHNICAL TRANSLATIONS: Information published in a foreign language considered to merit NASA distribution in English.

SPECIAL PUBLICATIONS: Information derived from or of value to NASA activities. Publications include conference proceedings, monographs, data compilations, handbooks, sourcebooks, and special bibliographies.

TECHNOLOGY UTILIZATION PUBLICATIONS: Information on technology used by NASA that may be of particular interest in commercial and other non-aerospace applications. Publications include Tech Briefs, Technology Utilization Reports and Notes, and Technology Surveys.

Details on the availability of these publications may be obtained from:

SCIENTIFIC AND TECHNICAL INFORMATION DIVISION
NATIONAL AERONAUTICS AND SPACE ADMINISTRATION
Washington, D.C. 20546